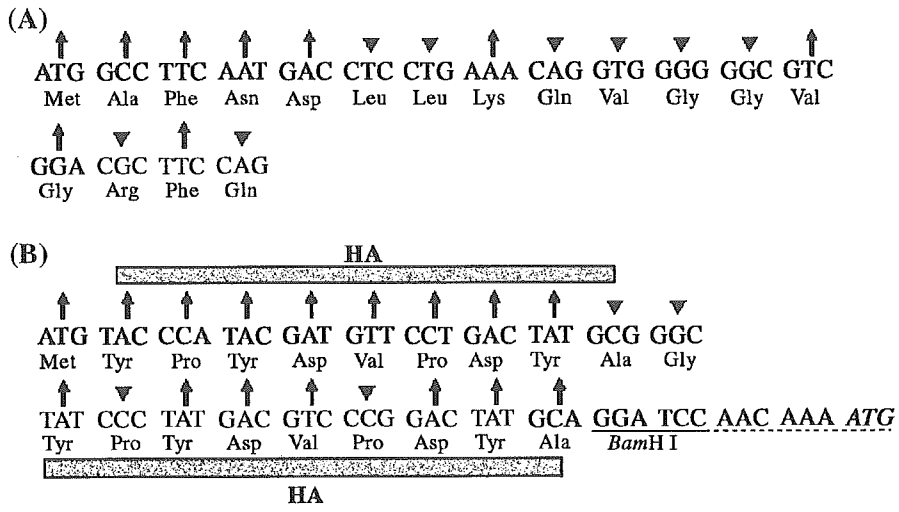

Fig. 1. The first 17 codons encoding the N-terminus of rOAT1 (A). The HA-epitope and the fusion site (B). ↑ represents codon preferred by yeast, ▼ indicate a non-preferred codon, *Bam*HI site is underlined and dot letters show a Kozak consensus sequence upstream of the rOAT1 start codon (italic). Open bars represents boundary of the HA-epitope.

Foreseeable problems with expression of mammalian membrane proteins in *S. cerevisiae* are the strong codon usage bias in yeast and differences in post-translational modification between yeast and mammalian systems, especially for glycosylation. Examination of codon usage at the 5′ end of rOAT1 revealed a trend of yeast non-favored codons. To overcome this problem, we used the strategy of constructing HArOAT1 (Fig. 1) to contain the readily translatable HA (hemagglutinin) epitope fused upstream of the rOAT1 start codon.

To find a suitable expression system for rOAT1, the HA-fusion rOAT1 gene was cloned into different yeast expression plasmids, both integrative and multicopy, with the constitutive *ADH1* promoter or the *GAL1* inducible promoter. The effect of growth temperature on glycosylation of yeast-expressed rOAT1 was also studied. In addition, the transport ability and plasma membrane targeting of the protein were examined to determine whether heterologously expressed rOAT1 retained structural and functional characteristics.

2. Materials and methods

2.1. Vector constructions

rOAT1 *cDNA (accession number: AB004559*, GenBank™ nucleotide data bases) was kindly provided by Prof. H. Endou (Kyorin University, Japan) in plasmid pSPORT1. The rOAT1 ORF was previously cloned into pBlueScript SK between the *Bam*HI and *Eco*RI sites to yield pBPII (B. Punlungka unpublished data). The *Bam*HI–*Eco*RI cDNA fragment for rOAT1 was extracted from pBPII and inserted into pFA6a–*TRP1*–*pGAL1*–3HA (obtained from Dr. H. Qui, NIH). The newly constructed plasmid named pFA6a–*TRP1*–*pGAL1*–HArOAT1 harbored the rOAT1 ORF modified at the translation initiation region by fusion with two copies of the HA encoding sequence.

The HA–rOAT1 fusion gene (HArOAT1) was amplified by PCR using a forward primer designed to introduce the sequence TTAGAGCTC*AA*AATG (*Sac*I site underlined, Kozak consensus sequence in italics) to the 5′ end and a reverse primer designed for addition of an *Eco*RI site immediately downstream of the stop codon. The resulting blunt-end PCR fragment was digested with *Eco*RI, to generate a 3′ *Eco*RI cohesive end before it was ligated into pSP72 vector between *Eco*RI and *Eco*RV restriction sites. The correct sequence of the PCR amplified HArOAT1 gene could then be confirmed by DNA sequencing using T7 and SP6 primers. The *Sac*I restriction site of pSP72 located next to the *Eco*RI cloning site could be utilized for subcloning the gene into several expression plasmids. Since the PCR product was rather long, only the modified N- and C-terminal sequences were verified by a single pair of primers. Finally, the middle fragment from the *Bst*EII to *Nhe*I site of the PCR-amplified HArOAT1 was replaced with the original HArOAT1 cDNA from PBPII to yield plasmid pSP72–HArOAT-1.

The parent vector for construction of an integrative HArOAT1 expression plasmid was generated from insertion of an *ADH1* promoter-multicloning site-*CYC1* terminator cassette from pTB326 vector (kindly provided by Dr. H. Qui, NIH) into the integrative vector YIPBssHII 211 (obtained from Dr. J. Hauf, Technical University of Darmstadt, Germany). To facilitate subcloning of genes, some restriction sites in YIPBssHII 211 corresponding to the multicloning site of pTB326 firstly had to be removed. YIPBssHII 211 was digested with *Bam*HI and *Eco*RI to cleave out *Sac*I, *Kpn*I and *Sma*I restriction sites, then treated with Mung bean nuclease to destroy *Bam*HI and *Eco*RI restriction sites. The blunt ends of the linearized plasmid were then ligated together before insertion of the *Sph*I–*Xba*I fragment of the promoter–terminator cassette from pTB326, yielding the integrative yeast expression plasmid YIP211-1a. Then, the *Sac*I fragment of HArOAT1 from pSP72–HArOAT1-1 was ligated into the parent vector YIP211-1a to create the HArOAT1 integrative plasmid pSSI (Fig. 2). By ligation of the same fragment into pTB326, the HArOAT1 multicopy plasmid pSSIV (Fig. 2) was obtained. The multicopy plasmid pSSIII (Fig. 2) for *GAL1*-inducible expression of HArOAT1 was generated by insertion of the gene fragment extract from pSP72–HArOAT1-1 into pYES2 vector (Invitrogen) between *Eco*RI and *Sac*I sites. The wild type rOAT1 gene extracted from pBPII by digestion with *Bam*HI and *Eco*RI was also cloned into pYES2 to yield plasmid pSSII (Fig. 2).

2.2. Strains and media

Escherichia coli strain DH5α (*F*φ80*dlac*ZΔ(*lac*ZYA–*arg*F)u169 deoR, *rec*A1, *end* A1, *hsd*R17(r_K^-, m_{K+}), *Sup*E44, λ-*thi*-1,*gyr*A96, *rec*1A1) was used for all bacterial work. The *S. cerevisiae* protease deficient strain BJ5462 (*MAT*α, *ura*3–5, *trp*1 *leu*2Δ1, *his*3Δ200, *pep*4::*HIS*3, *prb*1Δ1 1.6R, *can*1, *GAL*) (Yeast Genetic Stock Center, University of California) was used throughout the study. Untransformed yeast cells were grown in SD minimal medium containing 0.67% (w/v) yeast nitrogen base without amino acids (DIFCO Laboratories), 2% (w/v) D-glucose supplemented with an amino acid mixture. The same medium supplemented with an amino acid mixture lacking uracil or lacking tryptophan was used for growing cells transformed with

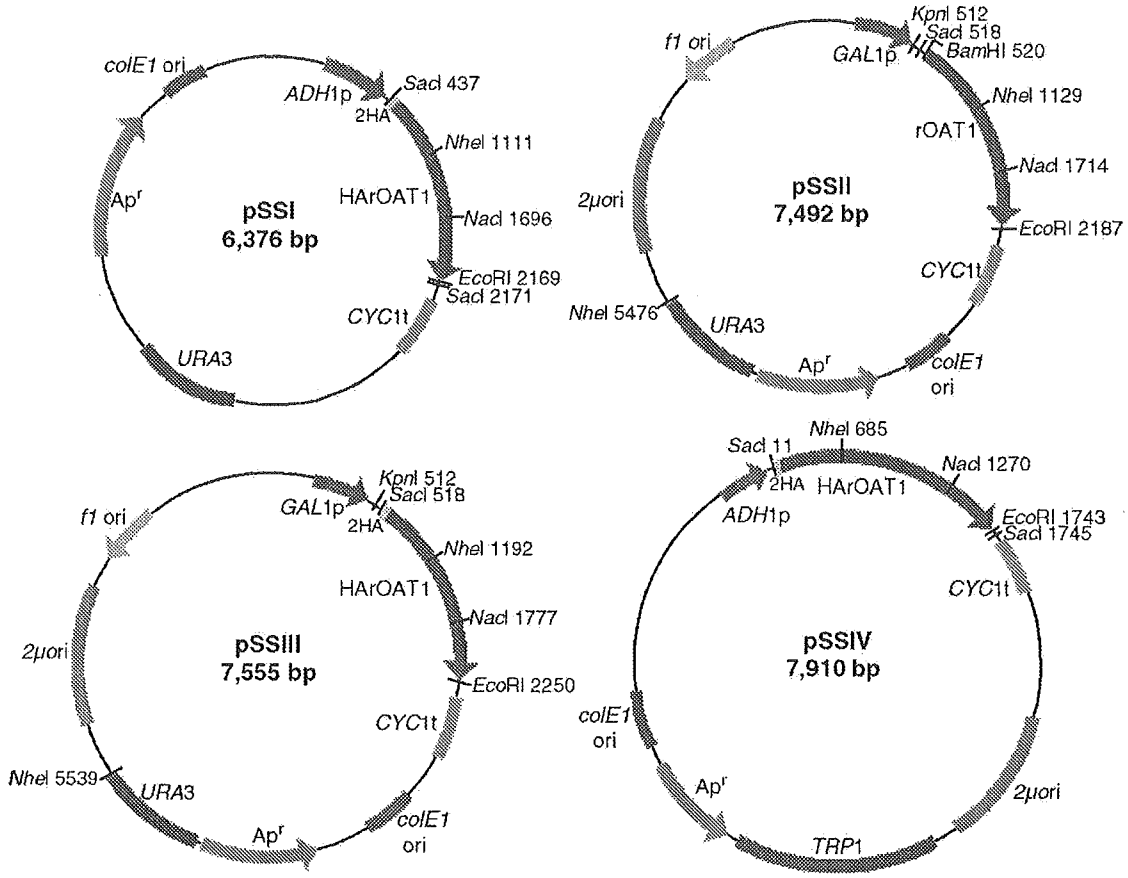

Fig. 2. Physical maps of rOAT1-expressing yeast plasmids. The integrative plasmid pSSI is *URA*3 selectable and encodes the HA-fusion rOAT1 under control of the constitutive *ADH*1 promoter. In the *TRP*1-selectable 2 μ plasmid pSSIV, expression of HArOAT1 is also controlled by *ADH*1 promoter. The galactose-inducible GAL1 promoter was used to control expression of HA-modified rOAT1 and wild type rOAT1 in the multicopy plasmid with *URA*3 selectable marker pSSIII and pSSII, respectively. *CYC*1 transcriptional terminator was used in all plasmids.

*URA*3 plasmid or *TRP*1 plasmid, respectively. Solid media contained an additional 2% (w/v) Bacto-Agar (DIFCO Laboratories).

2.3. Transformation and culture conditions

Yeast cells were transformed by the lithium acetate method described by I to [13] with some modifications [14]. Transformants were identified by auxotrophic selection. All experimental cultures were inoculated at an OD660 of 0.01 from actively growing pre-cultures. Throughout the experiments, cultivation of transformants for gene expression under control of the constitutive promoter *ADH*1 was performed using SD medium containing glucose as the sole carbon source. For inducible expression under control of *GAL*1 promoter, cells were grown in SD medium using 2% raffinose as the carbon source until OD660 reached 0.6–0.8 units (early exponential phase), at which time expression was induced by addition of galactose to a final concentration of 2%. Unless indicated otherwise, the cultures were allowed to grow at 30 °C with constant agitation (200 rpm).

2.4. Isolation of crude yeast membranes and plasma membranes

Yeast cells were grown as above, and crude cellular membranes were prepared by a glass bead lysis protocol [9]. Plasma membranes were purified by the acid precipitation method of Goffeau and Dufour [15]. Protein concentrations were measured by the Bradford method [16].

2.5. Deglycosylation

Endoglycosidase H deglycosylation of proteins was performed as described by Imamura [17] with some modifications. Five μl of 200 mM NaH_2PO_4, pH 5.5 and 0.2% (w/v) SDS were added to 20 μg proteins from yeast plasma membrane extracts. Then 10 mU of endoglycosidase H was added and samples were incubated for 12 h at 37 °C.

2.6. Western blots

Twenty μg protein samples were subjected to 10% SDS-PAGE gel and run at 110 V for about 2 h, followed by transfer onto polyvinylidene difluoride membranes at 0.1 Amp overnight. The membranes were then washed with TBST (20 mM Tris–HCl pH 7.5, 150 mM NaCl and 0.05% (v/v) Tween 20) for 30 min, blocked with 5% skim milk in TBST for 1 h with agitation. Afterward, membranes were incubated with anti-OAT1 rabbit polyclonal antibody (1:5000 dilution) or anti-HA mouse monoclonal antibody (1 μg/ml), for 3 h with gentle agitation. After washing 3 times in TBST (5 min each), membranes were incubated in 1:5000 dilution of anti-rabbit or anti-mouse IgG AP conjugated for 1 h with gentle agitation, washed 3 times in TBST and 2 times in TBS (20 mM Tris–HCl pH 7.5 and 150 mM NaCl) to remove Tween 20. The BCIP/NBT kit (Zymed) was employed for protein detection.

2.7. Anion transport assay

Recombinant cells were cultured for expression of rOAT1 as described above, harvested at mid exponential phase (*GAL*1 inducible expression) or late exponential phase (*ADH*1 constitutive expression), and washed once with Dulbecco's phosphate buffer saline (137 mM NaCl, 3 mM KCl, 1.5 mM KH_2PO_4, 8 mM Na_2HPO_4, 1 mM $CaCl_2$, and 0.5 mM $MgCl_2$) supplemented with 0.15 M D-glucose [9], pH 7.4 that was also used as transport buffer. The cells were then resuspended to 68 $OD_{660} \times 20\ \mu l^{-1}$ for one reaction with the same buffer containing 1 mM glutarate in the presence or absence of 2 mM probenicid

and incubated for 1 h at room temperature. After washing 3 times with the same buffer, uptake experiments were initiated by rapidly mixing 20 μl of cell suspension with 80 μl of transport buffer containing 2 μM [^{14}C]PAH (0.1 mCi/ml). At specific times, reactions were stopped by addition of 1 ml ice-cold transport buffer and the cells were trapped by filtering through Whatman GF/C filters. The filters were washed five times with 1 ml ice-cold transport buffer and trapped radioactivity was quantified by liquid scintillation spectrometry.

3. Results

3.1. rOAT1 is expressed in yeast only when HA is fused preceding its N-terminus

Examination of codon usage at the 5′ end of rOAT1 revealed that the first 17 codons encoding the N-terminus included at least 8 codons seldom used in yeast for highly expressed proteins (Fig. 1). To test whether an intrinsic determinant within the gene impeded rOAT1 expression, 21 codons encoding 2 copies of HA epitope were fused in frame preceding the start codon of rOAT1. This created HArOAT1 that contained only 4 yeast non-favored codons.

Since expression of foreign membrane proteins may interfere with cellular process and may affect cell growth and viability, the HA-modified rOAT1 gene was cloned into different yeast expression plasmids that allowed control of expression levels. As detailed in Materials and methods, four types of plasmids were constructed. All plasmids were introduced by transformation into yeast strain BJ5462. Expression of rOAT1 in the yeast plasma membrane fraction was assessed by Western blot using polyclonal antibody directed against the carboxy terminus of the transporter. No immunoreactive material was detected in plasma membrane prepared from any control strains transformed with parental plasmids YIP211-1a, pTB326 or pYES2 (Fig. 3 lanes 1, 2, 3), or in the strain that carried the wild type rOAT1 expression plasmid pSSII (Fig. 3 lane 4). Addition of HA to the 5′ end changed the expression of rOAT1. The HA-fusion rOAT1 protein encoded by pSSI, pSSIV and pSSIII (Fig. 3 lanes 5, 6, 7) migrated on SDS-PAGE with apparent molecular masses of 60–88 kDa, which was in good agreement with the molecular mass rOAT1 predicted from the amino acid sequence (60 kDa) [2,7,18] and with the molecular mass of glycosylated rOAT1 protein detected in rat kidney with the same antibody (77.8 kDa) [19]. These results indicated the importance of codons at the N-terminus for expression of rOAT1. By N-terminal fusion of short sequence encoding yeast-favored codons, rOAT1 was able to be expressed in yeast. Furthermore, as determined by signal intensity, the highest expression level of HArOAT1 came from *GAL1* inducible promoter in the high copy plasmid pSSIII; while the constitutive promoter *ADH1* in the integrative plasmid pSSI showed the least expression level. The same result was also observed when Western blot was performed using mouse monoclonal antibody against HA epitope (data not shown). The small proteins found in the rOAT1-expressed strains might come from protease degradation of rOAT1. This was supported by a large number of predicted proteasomal cleavage sites in rOAT1 protein.

Influenza virus hemagglutinin has a signal peptide that mediates translocation of the protein across the endoplasmic reticulum (ER) membrane. Addition of this transport signal

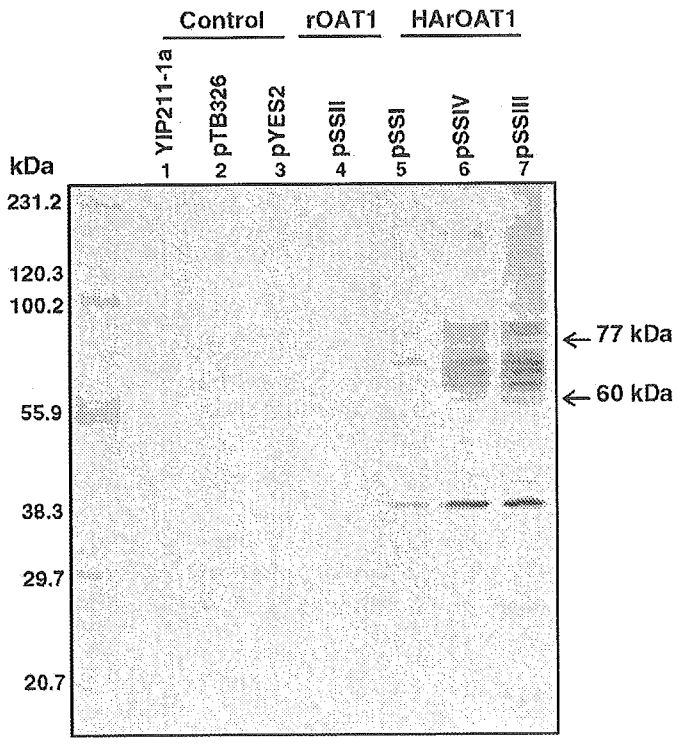

Fig. 3. Expression of the N-terminal modified rOAT1 in yeast. Plasma membranes were prepared from yeast cells with only empty vector YIP211-1a, pTB326 or pYES2; with the wild type rOAT1 plasmid pSSII; and with the HA-fusion rOAT1 (HArOAT1) plasmid pSSI, pSSIV, pSSIII. 20 μg proteins from each sample were subjected to SDS-PAGE and immunoblotted with polyclonal antibody raised against C-terminus of rOAT1.

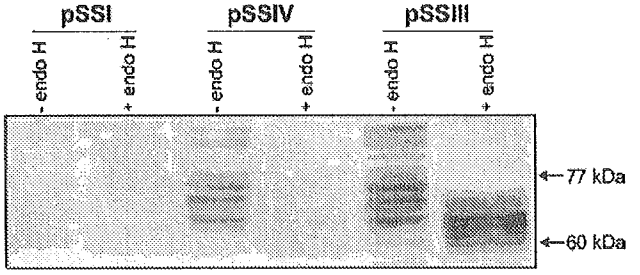

Fig. 4. rOAT1 is glycosylated in yeast. 20 μg endo H-treated and untreated proteins from the cells carrying plasmid pSSI, pSSIV, or pSSIII grown at 30 °C and 16 °C (A) as compared with the 16 °C-growing cells (B), were detected by Western blot using monoclonal antibody against HA epitope.

from hemagglutinin to the N-terminus of yeast protein carboxypeptidase Y (CPY) efficiently directed the protein to the ER in a mammalian expression system [20]. In silico prediction of subcellular localization suggested that 66.7% of the wild type rOAT1 was located in the ER and only 33.3% in the plasma membrane. HA insertion apparently changed the predicted localization of rOAT1. An almost 2-fold increase in plasma membrane targeting (65.2%) was predicted for the HA-fusion protein and only small fractions should have been seen in the ER, Golgi cisternae, vacuolar membranes and nuclear membrane. Immunoblots of total cellular extract with both OAT1 and HA antibody (data not shown) showed the same banding pattern as observed with the plasma membrane. Detection of rOAT1 protein was only in the total cell extract of the HA-rOAT1 recombinant yeast confirmed the role of HA in the enhancement of rOAT1 expression rather than plasma membrane targeting.

3.2. rOAT1 is glycosylated in yeast, unaffected by growth temperature

The native rat OAT1 is glycosylated with up to 17 kDa of carbohydrate [2]. It has been suggested that this carbohydrate is required for sorting of OAT1 to the plasma membrane. Many mammalian membrane proteins expressed in yeast are not glycosylated [9,21–23]. To determine whether the yeast-expressed rOAT1 was glycosylated, plasma membrane isolated from three rOAT1 recombinant strains were treated with enzyme endoglycosidase H, which cleaves the entire high mannose and some hybrid oligosaccharide structure at the glucosamine linkage of N-linked carbohydrates. Immunoblot analysis using the anti-HA monoclonal antibody showed that upon treatment with endoglycosidase H, the electrophoretic mobility of rOAT1 was altered. The apparent molecular masses from over 60 kDa to 88 kDa were reduced mostly to the unglycosylated size of 60 kDa after deglycosylation (Fig. 4). These results indicated that a large fraction of rOAT1 was glycosylated at several levels in yeast.

It has been suggested that an important function of N-linked glycosylation is the quality control for correct protein folding in the endoplasmic reticulum (ER) [24]. Since protein folding and stability often favor low temperatures, glycosylation of rOAT1 in yeast grown at low temperature was investigated. The similar band pattern in immunoblot of the plasma membrane prepared from rOAT1 recombinant strains grown at 30 °C and 16 °C both before and after endoglycosidase H treatment (Fig. 4) indicated the unaltered glycosylation at different temperatures.

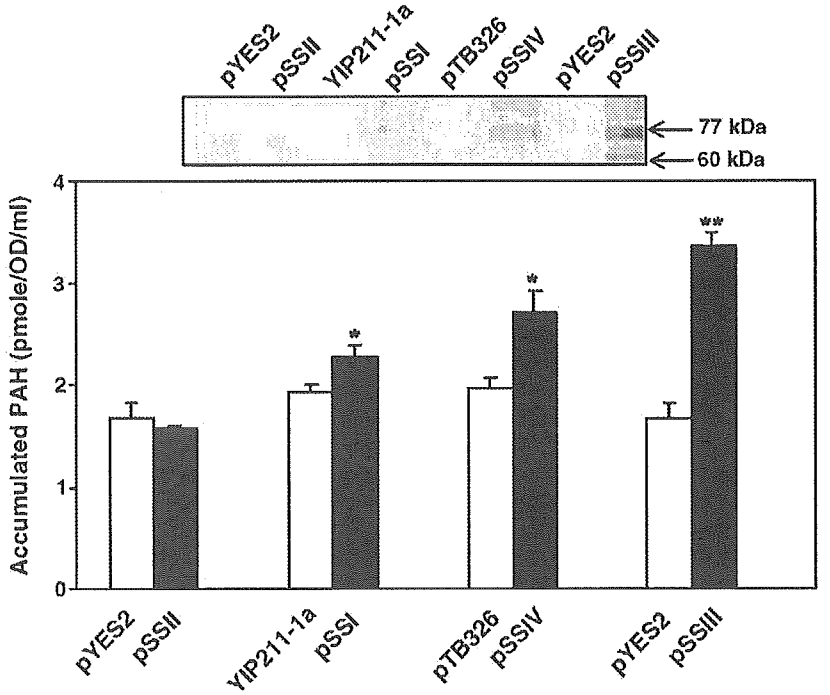

Fig. 5. The rOAT1 expressed in yeast is in functional form [^{14}C] PAH uptake into yeast cells carrying plasmid pSSII and into the rOAT1 expressing cells carrying plasmid pSSI, pSSIV or pSSIII are compared with the uptake in control cells with parent vectors YIP211-1a, pTB326 or pYES2. Each column represents the mean ± S.E. value of accumulated [^{14}C] PAH measured for 10 min in three independent experiments. *$P<0.05$; **$P<0.01$ indicate significant differences from controls.

3.3. Yeast-expressed rOAT1 is able to transport p-aminohippurate (PAH)

To assess the capability of the yeast-expressed rOAT1 to mediate organic anion exchange, the model substrate PAH was chosen. rOAT1 recombinant strains and control strains carrying only parent vector were cultured for either constitutive or inducible expression of rOAT1. The cells were then loaded with 20 μM [^{14}C] PAH and assayed for anion uptake by measuring the influx of radioactive PAH in exchange for intracellular glutarate [6] (Fig. 5). No apparent difference in the PAH uptake was observed between cells with the wild type rOAT1 plasmid pSSII and those with pYES2 (control cells). By contrast, recombinant yeast carrying the high copy plasmid pSSIV showed very much higher PAH uptake) than control cells carrying parent vector pTB326. Cells carrying pSSIII (highest expression of rOAT1) showed a 2-fold increase in PAH uptake when compared to pYES2-carrying cells. There was a positive correlation between rOAT1 expression level (determined by intensity of 60–88 kDa bands detected in Western blots) and PAH uptake ability in each recombinant strain.

An inhibition study was also performed in order to confirm the specificity of PAH transport by heterologously expressed rOAT1. In the presence of 2 mM probenecid, a classical inhibitor of the uptake system, the amount of PAH taken up by all HArOAT1 recombinant strains was substantially reduced (Table 1). Accumulated PAH in control cells that showed no detectable level of rAOT1 was also reduced in the presence of probenecid. Many intrinsic yeast anion transporters are known to have wide ranges of substrate specificity. The inhibition study suggested that the host yeast *S. cerevisiae* strain BJ5462 had its own transport mechanism for PAH and that probenecid was also able to inhibit that system (Table 1).

3.4. rOAT1 targets plasma membrane

Previous functional assays supported the possibility that rOAT1 is expressed at the cell surface where it mediates PAH entrance into cells. To determine the location of rOAT1 in recombinant yeast strains, Western blot analysis of various cellular fractions was performed (Fig. 6). In all rOAT1 recombinant strains, the greatest amount of rOAT1 protein was detected in the plasma membrane. The same quantity of protein from crude membrane fractions that included both plasma membranes and organelle membranes showed lower levels of rOAT1. A relatively small amount of the transporter was found in the soluble fraction. Interestingly, the presence of only the unglycosylated protein (60 kDa) in the intracellular fluid (i.e., soluble fraction) is in agreement with the suggestion that glycosylation is important for OAT1 targeting to the plasma membrane.

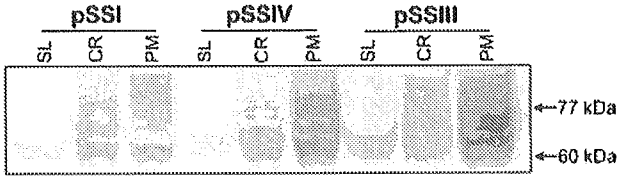

Fig. 6. Localization of rOAT1 in yeast cells. Western blot of plasma membranes (PM), crude cellular membranes (CR), and soluble fractions (SL) prepared from rOAT1 recombinant strains carrying plasmid pSSI, pSSIV and pSSIII, using monoclonal antibody against HA epitope. Each lane contains 20 μg of protein.

4. Discussion

The present study demonstrated that codon usage at the N-terminus of the rat organic anion transporter 1 (rOAT1) is important for the successful expression of rOAT1 in the yeast *S. cerevisiae*. The use of synonymous codons in *S. cerevisiae* is strongly biased [25], mostly due to abundances of different tRNA species [26] and it has been suggested that the efficiency of protein synthesis is increased when required tRNA are not limited. In addition, translation efficiency may also affect the stability of the mRNA transcript. Preferred codons therefore improve both transcriptional and translational processes in protein expression [10]. By synthesizing an ideal gene with yeast preferred codons, successful expression of malarial parasite integral membrane protein Pfcrt in yeast was achieved [27]. Study on the role of biased codon usage in expression of phoshoglycerate kinase (*PGK1*) gene [28] showed that replacement of major codons at the 5′ end of the coding sequence with synonymous minor ones, substantially decreased expression. Instead of substituting minor codons with major codons, we fused an HA sequence consisting of mostly yeast-preferred codons preceding the start codon of rOAT1 in order to simplify initiation of translation. We found that rOAT1 was expressed in yeast with this modification only (Fig. 3). This method has proven useful in a previous study on expression of rat and bovine vesicular monoamine transporters (rVMAT1 and bVMAT2, respectively) in yeast [10]. In addition, we found that the best rOAT1 expression was obtained with a multicopy plasmid in which the expression was controlled by the inducible promoter *GAL1* (Fig. 3).

The apparent sizes of the yeast-expressed rOAT1 varied from 60 to 88 kDa. Treatment with endoglycosidase H demonstrated that those proteins of over 60 kDa were glycosylated (Fig. 4). Although *S. cerevisiae* is able to glycosylate proteins, it has been shown that oligosaccharide

Table 1
Amount of [^{14}C] PAH accumulated in recombinant yeasts in the presence and absence of 2 mM probenicid

PAH uptake (pmole/OD/ml) Recombinant yeast carrying plasmid	YIP211-1a	pYES2	pTB326	pSSI	pSSII	pSSIII	pSSIV
Without Probinicid	1.932±0.07	1.672±0.15	1.965±0.11	2.260±0.11	1.566±0.02	3.351±0.12	2.693±0.22
With Probinicid	0.145±0.07	0.221±0.19	0.108±0.05	0.182±0.13	0.228±0.12	0.184±0.04	0.324±0.15

Each value represents the mean±S.E from triplicate experiments. The paired results in each column were all significantly different ($P<0.001$) by Student's t test.

structures are significantly different from their authentic versions in mammalian cells [29,30]. Usually, yeast makes extensive mannosylation [31]. Since glycosylated rOAT1 found in the rat kidney is about 77 kDa [17], the larger protein detected in the yeast plasma membrane may have resulted from hypermannosylation.

The effect of cultivation temperature on protein expression and post-translational, modification has been reported for expression of rVMAT1 in yeast [10]. By lowering cultivation temperatures, expression of rVMAT1 was remarkably improved and the unglycosylated protein underwent core glycosylation. In contrast to rVMAT1, glycosylation and expression level of rOAT1 were the same at 30 °C and 16 °C.

Molecular mechanisms that determine membrane localization of proteins in *S. cerevisiae* are not well understood, but the same principles seem to govern membrane trafficking in yeast and higher eukaryotes. An important factor effecting membrane targeting is protein folding. Only proteins that are correctly folded leave the ER and move forward into the Golgi. Misfolded proteins undergo ER-associated degradation and the process involves dislocation of the cargo proteins followed by ubiquitination and proteolytic degradation [32]. Protein modification is associated with folding in the ER and glycosylation may be required for correct folding. Control of proper folding may be a major purpose of modifications. For example, inhibition of glycosylation has been demonstrated to lead to protein misfolding followed by degradation in the ER [32]. However, carbohydrate moieties have also been shown to serve as transport signals for targeting the plasma membrane. Unglycosylated, secretory rat growth hormone fused to the transmembrane and cytosolic domains of vesicular stomatitis virus G protein was blocked in the Golgi complex and unable to reach the plasma membrane. Insertion of N-glycosylation sites into an extracellular domain can enable a protein to target the cell surface [33]. In epithelial Madin-Darby Canine kidney cells, the glycosylated form of rat growth hormone was secreted through the apical membrane, whereas the nonglycosylated native form was randomly secreted both apically and basolaterally [34]. The role of O-glycosylation as a membrane transport signal has also been displayed in the study of the yeast integral membrane protein Fus1p that is involved in cell fusion during yeast mating [35]. Insertion of the Fus1 ectodomain containing several potential O-glycosylation sites between the N-terminal part of invertase and the transmembrane domain of Fus1p altered the localization of the chimeric protein and it accumulated extracellularly. In the mutant yeast pmt4Δ that is unable to glycosylate proteins, the chimeric protein was blocked in the Golgi complex.

The role of N-linked glycosylation in plasma membrane targeting of OAT1 has been clearly demonstrated. Removal of all N-glycosylation sites from mouse and human analogs of OAT1 (mOAT1 and hOAT1, respectively) by replacing asparagine with a glutamine residue resulted in failure to target to the plasma membrane and accumulation intracellular compartments [36]. This was in good agreement with previous results of the same group showing that treatment of mOAT1-expressing COS-7 cells with tunicamycin to inhibit N-linked glycosylation resulted in failure of protein translocation to the plasma membrane [37]. Examination of rOAT1 localization in recombinant yeasts strongly supports these results. Glycosylated OAT1 was found exclusively in the yeast plasma membrane while the unglycosylated protein was found in the intracellular fluid (Fig. 6).

The possible cellular mechanisms underlying the function of carbohydrate moieties that determine apical transport of glycoproteins in epithelial cells have been proposed. One model suggests that hypothetical lectins bind to the glycans and bring the glycoproteins to transport carriers in the trans-Golgi network [34]. Another model suggests that glycans change the biophysical properties of proteins to facilitate the presentation of sorting signals to their receptors [35,38].

The ability of hetorologously expressed rOAT1 to transport PAH indicated that the structure and function of the transporter was at least partially preserved in *S. cerevisiae* (Fig. 5). PAH transport by proximal tubules in the rat kidney has been examined by various methods, including the stopped flow capillary perfusion method. PAH was transported into proximal tubular cells with a K_m of 0.08 ± 0.01 mM and Vmax of 1.1 ± 0.1 pmol $\times s^{-1} \times cm^{-1}$ [39]. Comparison of the transport ability of yeast-expressed rOAT1 with the native protein in the rat kidney requires purification and reconstitution of the protein into synthetic vesicles for further study of transport kinetics. In addition, it has been reported that transport function of mOAT1 and hOAT1 was almost completely lost when the putative glycosylation site Asp-39 was disrupted. However, it was found that this putative site was used for glycosylation only in hOAT1 and not in the mouse homolog. In addition, disruption of other putative glycosylation sites in both proteins had no effect on the transport activity of either mOAT1 or hOAT1 [36]. The transport function of heterologously expressed rOAT1 in this study was assessed using a whole cell transport assay, in which only the function of the plasma membrane inserted rOAT1 could be examined.

In summary, we reported the first successful expression of functional rOAT1 protein in yeast. This will lead the way to further studies on molecular structure and transport mechanisms and perhaps eventually to the development of in vitro systems for studying drug kinetics or for screening drug nephrotoxicity.

Acknowledgements

We would like to thank Prof. Yoshikatsu Kanai for their generosity providing rOAT1 cDNA and anti-OAT1 antibody. We thank Dr. Qui Hongfang for a kind gift of plasmid pFA6a–*TRP1*–*pGAL1*–3HA and pTB326, and Dr. Jörg Hauf for providing plasmid YIPBssHII 211. The authors would also like to thank Prof. Timothy Flegel for critical reading of the manuscript.

References

[1] R.A.M.H. Van Aubel, R. Masereeuw, F.G.M. Russel, Molecular pharmacology of renal organic anion transporters, Am. J. Physiol. Renal. Physiol. 279 (2000) F216–F232.

[2] T. Sekine, S.H. Cha, H. Endou, The mulispecific organic anion transporter (OAT) family, Pflügers Arch. 440 (2000) 337–350.
[3] D.H. Sweet, J.B. Pritchard, The molecular biology of renal organic anion and organic cation transporters, Cell Biochem. Biophys. 31 (1999) 89–118.
[4] G. Burckhardt, N.A. Wolff, Structure of renal organic anion and cation transporters, Am. J. Physiol. Renal. Physiol. 278 (2000) F853–F866.
[5] G. Burckhardt, A. Bahn, A.N. Wolff, Molecular physiology of renal p-aminohippurate secretion, News Physiol. Sci. 16 (2001) 114–118.
[6] T. Sekine, N. Watanable, M. Hosoyamada, Y. Kanai, H. Endou, Expression cloning and characterization of a novel multispecific organic anion transporter, J. Biol. Chem. 272 (1997) 18526–18529.
[7] D.H. Sweet, N.A. Wolff, J.B. Pritchard, Expression cloning and characterization of ROAT1, the basolateral organic anion transporter in rat kidney, J. Biol. Chem. 272 (1997) 30088–30095.
[8] G.L. Kiser, M. Gentzsch, A.K. Kloser, E. Balzi, D.H. Wolf, A. Goffeau, J.R. Riordan, Expression and degradation of the cystic fibrosis transmembrane conductance regulator in *Saccharomyces cerevisiae*, Arch. Biochem. Biophys. 390 (2001) 195–205.
[9] F. Fritz, E.M. Howard, M.M. Hoffman, P.D. Roepe, Evidence for altered ion transport in *Saccharomyces cerevisiae* overexpressing human MDR 1 protein, Biochemistry 38 (1999) 4214–4226.
[10] R. Yelin, S. Schuldiner, Vesicular monoamine transporters heterologously expressed in the yeast *Saccharomyces cerevisiae* display high-affinity tetrabenazine binding, Biochim. Biophys. Acta 1510 (2001) 426–441.
[11] B. Anderson, R.C. Stevens, The human D_{1A} dopamine receptor: heterologous expression in *Saccharomyces cerevisiae* and purification of the functional receptor, Protein Expr. Purif. 13 (1998) 111–119.
[12] R. Wieczorke, S. Dlugai, S. Krampe, E. Boles, Characterisation of mammalian GLUT glucose transporters in a heterologous yeast expression system, Cell. Physiol. Biochem. 13 (2003) 123–134.
[13] Y. Itoh, Y. Fukuda, K. Murata, A. Kimura, Transformation of intact yeast cells treated with alkaline cations, J. Bacteriol. 153 (1983) 163–168.
[14] D. Gietz, A. St. Jean, P.A. Woods, R.H. Schiestl, Improved method for high efficiency transformation of intact yeast cell, Nucleic Acids Res. 20 (1991) 1425.
[15] A. Goffeau, J.-P. Dufour, Plasma membrane ATPase from the yeast *Saccharomyces cerevisiae*, Methods Enzymol. 157 (1988) 528–533.
[16] M.M. Bradford, A rapid and sensitive method for the quantitation of microgram quantities of protein utilizing the principle of protein-dye binding, Anal. Biochem. 72 (1976) 248–254.
[17] K. Imamura, M. Araki, A. Miyanohara, J. Nakao, H. Yonemura, N. Ohtomo, K. Matsubara, Expression of hepatitis B virus middle and large surface antigen genes in *Saccharomyces cerevisiae*, J. Virol. 61 (1987) 3543–3549.
[18] M. Ljubojeviæ, M.C. Herak-Kramberger, Y. Hagos, A. Bahn, H. Endou, G. Burckhardt, I. Sabolic, Rat renal cortical OAT1 and OAT3 exhibit gender differences determined by both androgen stimulation and estrogen inhibition, Am. J. Physiol. Renal Physiol. 287 (2004) F124–F138.
[19] N. Nakajima, T. Sekine, S.H. Cha, A. Tojo, M. Hosoyamada, Y. Kanai, K. Yan, S. Awa, H. Endou, Developmental changes in multispecfic organic anion transporter 1 (OAT1) expression in the rat kidney, Kidney Int. 57 (2000) 1608–1616.
[20] P. Bird, M.-J. Gething, J. Sambrook, Translocation in yeast and mammalian cells: not all signal sequences are functionally equivalent, J. Cell Biol. 105 (1987) 2905–2914.
[21] K. Kuchler, J. Thorner, Functional expression of human mdr1 in the yeast *Saccharomyces cerevisiae*, Proc. Natl. Acad. Sci. 89 (1992) 2302–2306.
[22] I. Sekler, R. Kopito, J.R. Casey, High level expression, purification, and functional reconstitution of the human AE1 anion exchanger in *Saccharomyces cerevisiae*, J. Biol. Chem. 270 (1995) 21028–21034.
[23] R.A. Figler, H. Omote, R.K. Nakamoto, M.K. Al-Shawi, Use of chemical chaperones in the yeast *Saccharomyces cerevisiae* to enhance heterologous membrane protein expression: high-yield expression and purification of human p-glycoprotein, Arch. Biochem. Biophys. 376 (2000) 34–46.
[24] E.S. Trombetta, A. Helenius, Lectins as chaperones in glycoprotein folding, Curr. Opin. Struct. Biol. 8 (1998) 587–592.
[25] J.L. Bennetzen, B.D. Hall, Codon selection in yeast, J. Biol. Chem. 257 (1982) 3026–3031.
[26] M. Bulmer, Coevolution of codon usage and transfer RNA abundance, Nature 325 (1987) 728–730.
[27] H. Zhang, E.M. Howard, P.D. Roepe, Analysis of the antimalarial drug resistance protein Pfcrt, J. Biol. Chem. 277 (2002) 49767–49775.
[28] A. Hoekema, R.A. Kastelein, M. Vasser, H.A. de Boer, Codon replacement in the PGK1 gene of *Saccharomyces cerevisiae*: experimental approach to study the role of biased codon usage in gene expression, Mol. Cell. Biol. 7 (1987) 2914–2924.
[29] M.A. Kekuruzinska, M.L.E. Bergh, B.L. Jackson, Protein glycosylation in yeast, Annu. Rev. Biochem. 56 (1987) 915–944.
[30] R. Kornfeld, S. Kornfeld, Assembly of asparagine-linked oligosaccharide, Annu. Rev. Biochem. 54 (1985) 631–664.
[31] M. Rai, H. Padh, Expression systems for production of heterologous proteins, Curr. Sci. 80 (2001) 1121–1128.
[32] R.Y. Hampton, ER-associated degradation in protein quality control and cellular regulation, Curr. Opin. Cell Biol. 14 (2002) 476–482.
[33] J.L. Guan, C.E. Machamer, J.K. Rose, Glycosylation allows cell surface transport of an anchored secretory protein, Cell 42 (1985) 489–496.
[34] P. Scheiffele, J. Peranen, K. Simons, N-glycans as apical sorting signals in epithelial cells, Nature 378 (1995) 96–98.
[35] T.J. Proszynski, K. Simons, M. Bagnat, O-glycosylation as a sorting determinant for cell surface delivery in yeast, Mol. Biol. Cell 15 (2004) 1533–1543.
[36] K. Tanaka, W. Xu, F. Zhou, G. You, Role of glycosylation in the organic anion transporter OAT1, J. Biol. Chem. 279 (2004) 14961–14966.
[37] K. Kuze, P. Graves, A. Leahy, P. Wilson, H. Stuhlmann, G. You, Heterologous expression and functional characterization of a mouse renal organic anion transporter in mammalian cells, J. Biol. Chem. 274 (1999) 1519–1524.
[38] E. Rodriguez-Boulan, A. Gonzalez, Glycans in post-Golgi apical targeting: sorting signals or structural props? Trends Cell Biol. 9 (1999) 291–294.
[39] K.J. Ulrich, G. Rumrich, G. Fritzsch, S. Kloss, Contraluminal para-aminohippurate (PAH) transport in the proximal tubule of the rat kidney: I. Kinetics, influence of cations, anions, and capillary preperfusion, Pflügers Arch. 409 (1987) 229–235.

Available online at www.sciencedirect.com
SCIENCE DIRECT
Biochimica et Biophysica Acta 1740 (2005) 29–37
BIOCHIMICA ET BIOPHYSICA ACTA
BBA
http://www.elsevier.com/locate/bba

Altered renal elimination of organic anions in rats with chronic renal failure

Adriana Mónica Torres[b,*], Myriam Mac Laughlin[a], Angélica Muller[a], Anabel Brandoni[b], Naohiko Anzai[c], Hitoshi Endou[c]

[a]*Instituto de Investigaciones Cardiológicas, Facultad de Medicina, Universidad de Buenos Aires, Argentina*
[b]*Farmacología, Facultad de Ciencias Bioquímicas y Farmacéuticas, Universidad Nacional de Rosario, CONICET, Argentina*
[c]*Department of Pharmacology and Toxicology, Kyorin University School of Medicine, Tokyo, Japan*

Received 23 September 2004; received in revised form 28 February 2005; accepted 1 March 2005
Available online 17 March 2005

Abstract

The progress of chronic renal failure (CRF) is characterized by the development of glomerular and tubular lesions. However, little is known about the expression of organic anions renal transporters. The objective of this work was to study, in rats with experimental CRF (5/6 nephrectomy), the expression of the organic anion transporter 1 (OAT1) and organic anion transporter 3 (OAT3) and their contribution to the pharmacokinetics and renal excretion of *p*-aminohippurate (PAH). Two groups of animals were used: Sham and CRF. Six months after surgery, systolic blood pressure and plasma creatinine concentrations were significantly higher in CRF groups. CRF rats showed a diminution in: the filtered, secreted and excreted load of PAH; the systemic clearance of PAH; the renal OAT1 expression; and the renal Na–K-ATPase activity. No remarkable modifications were observed in the OAT3 expression from CRF kidneys. The diminution in the systemic depuration and renal excretion of PAH may be explained by the decrease in its filtered and secreted load. The lower OAT1 expression in remnant renal mass of CRF rats or/and the lower activity of Na–K-ATPase might justify, at least in part, the diminished secreted load of this organic anion.

Keywords: Organic anion; Chronic renal failure; Renal depuration; Organic anion transporter 1; Organic anion transporter 3

1. Introduction

The progression of chronic renal failure (CRF) is characterized by the development of glomerular and tubular lesions about which multiple factors can be involved [1]. Regarding renal tubules, numerous studies have been performed to understand the pathological process [2], but it is less known about changes in tubular function. In the experimental model of subtotal nephrectomy, functional tubular changes and elevated filtration rate per remaining nephron are expected because of compensatory renal hypertrophy [3]. The increase per nephron of several tubular activities is proof of it [4]. Some authors have provided evidences that tubular dysfunction occurs in CRF [5–7]. It has been demonstrated that CRF induced a reduction in the expression and/or activity of several enzymes located in brush-border membranes and of type II Na–Pi cotransporter [5]. Other studies have also reported reduced expression per cellular unit of other enzymes or transporters present in the proximal and distal parts of the nephron [6,7].

The tubular secretion of organic anions is an important function of the kidney by eliminating potentially toxic organic anions from the body [8]. A number of drugs, such as β-lactamic antibiotics, diuretics, nonsteroidal anti-inflammatory drugs, and several antiviral drugs are also classified as organic anions, therefore, the renal organic anion transport system plays a key role in the pharmacokinetics of these drugs [8]. Organic anions are taken up from the

* Corresponding author. Suipacha 531, Rosario 2000, Argentina. Fax: +54 341 4371992.
E-mail address: adtorres@fbioyf.unr.edu.ar (A.M. Torres).

0925-4439/$ - see front matter © 2005 Elsevier B.V. All rights reserved.
doi:10.1016/j.bbadis.2005.03.002

peritubular plasma across the basolateral membrane and effluxed into the tubular fluid across the luminal membrane. The systems involved in organic anion secretion can be functionally subdivided in the well-characterized sodium-dependent *p*-aminohippurate (PAH) system and a recently discovered sodium independent system. Both systems mediate two membrane translocation steps arranged in series: uptake from blood across the basolateral membrane of renal epithelial cells, followed by efflux into urine across the apical membrane. A lot of organic anions transporters have been recently cloned. Among them, there were the organic anion transporter 1 (OAT1) and the organic anion transporter 3 (OAT3), which are considered the principal contributors to the classical renal organic anion secretory process [8–11]. Both OAT1 and OAT3 support OA/α-KG exchange [8]. PAH is a substrate for both rodent and human orthologs of OAT1 and OAT3 [8–11]. In the apical membrane, multidrug resistance protein 2 (MRP2) has been described as one of PAH transporters [12,13]. Recently, multidrug resistance protein 4 (MRP4) has been identified as a novel PAH transporter [14]. Organic anion transporters k1 and k2 (OAT-K1 and OAT-K2) are also present in luminal membrane of proximal tubule, but they do not transport PAH [15]. The functional and molecular changes in these organic ion transporters would result in impaired renal excretion of drugs, thereby causing unexpected adverse effects of administered ionic drugs. Whether drug secretion by renal tubules is modified in CRF is questioned because of frequent accumulation of various toxins in CRF. It is generally acknowledged that some anionic drugs should be used in lower dosages or with longer inter-dose intervals to prevent adverse effects in CRF. Thus, information regarding organic anion transporters (which play a significant role in their elimination) in CRF would be useful to determine the optimal use of drugs in progressive renal failure. In these regards, Laouari et al. [16] have found that CRF resulted in enhanced MRP2 expression, and Takeuchi et al. [17] have demonstrated that OAT-K1 and OAT-K2 expressions were depressed in CRF. As OAT1 and OAT3 also play an important role in renal drug secretion, the purpose of the present study was to examine the effects of chronic renal failure on the expression of OAT1 and OAT3 in rats, and the contribution of these effects on the pharmacokinetic and renal excretion of PAH.

2. Materials and methods

2.1. Experimental protocol

Two groups of rats were used: (1) Wistar rats that underwent sham operation with manipulation of pedicle (Sham). (2) Experimental chronic renal failure (CRF) was induced in male Wistar rats of 45 days old according to the technique of Morrison et al. [18] as we have previously described [19]. The two poles of the left kidney were removed and, 1 week later, the right kidney was excised. Rats of both groups were studied for 24 weeks starting at the time of right kidney uninephrectomy or sham operation.

2.2. Assays for chronic insufficiency development

Body weight and systolic blood pressure (SBP) were monitored weekly, and the plasma creatinine (PCr) concentrations were measured every week. SBP was measured in awake rats by tail plethismography as previously described [20,21]. PCr was measured by a modified Jaffe's method [22]. Histopathology of kidneys from Sham and CRF rats was performed after fixing in 10% neutral buffered formaldehyde solution for 4 h and embedding in paraffin, then 4 μm thick sections were processed for routine staining with hematoxylin and eosin.

2.3. Preparation of kidney homogenates

Kidneys from Sham ($n=4$) and CRF ($n=4$) were rapidly removed, the renal tissue was cleaned, dried, weighed, and placed in saline. Then, the tissue was thoroughly homogenized in 250 mM sucrose, 10 mM triethanolamine, and 0.1 mg/mL phenylmethylsulfonyl fluoride (PMSF). Protein quantification of samples was performed using the Sedmak and Grossberg method [23]. These homogenates were used for measuring alkaline phosphatase abundance and Na–K-ATPase activity.

2.4. Preparation of basolateral membrane (BLM)

The preparations of BLM from Sham and CRF rats were done by a modification of the method described by Jensen and Berndt [24] as previously reported by us [25,26]. Approximately 4 g of kidney tissue was placed in a Dounce homogenizer containing 50 mL of 250 mM sucrose, 5 mM Tris–Hepes pH 7.40. After four gentle strokes with the loose fitting pestle, the suspension was homogenized further with a motor-driven Teflon pestle (600 rpm/5 strokes) and spun down for 15 min at $1200 \times g$. The supernatant was aspirated and spun for 15 min at $22{,}000 \times g$. The fluffy beige upper layer of the resulting pellet (crude plasma membranes) was resuspended in about 1 mL of supernatant and added to 19 mL of buffered sucrose. The membrane suspension was homogenized gently through a 16-gauge gavage needle followed by the addition of 3.7 mL of 100% Percoll. The Percoll-membranes mixture was spun for 30 min at $39{,}250 \times g$. The top clear layer was discarded and the topmost dark band was removed. This layer was composed primarily of basolateral membranes as established by marker enzymes analysis. BLM were brought up in KCl buffer (85 mM KCl, 83 mM sucrose, 2 mM Hepes–Tris pH 7.40) at a ratio of 8 mL/g original wet weight. Then, BLM were pelleted at $30{,}000 \times g$ for 30 min and washed three times with the KCl buffer indicated. Finally, BLM were resuspended in 300 μL of 250 mM manitol, 10 mM Hepes–

Tris, pH 7.40. Aliquots of the membranes were stored immediately at −70 °C until use (no more than 2 weeks after membrane preparations). Each preparation represented renal tissue from six animals. Protein quantification of samples was performed using the method of Sedmak and Grossberg [23].

2.5. Immunoblot technique

Samples (Homogenates or BLM) were boiled for 3 min in the presence of 1% 2-mercaptoethanol/2% SDS (sodium dodecyl sulfate). Samples were applied to a 8.5% polyacrylamide gel, separated by SDS-PAGE, and then electroblotted to nitrocellulose membranes. For comparison between groups of animals, staining with ponceau red revealed that equal quantities of proteins were deposited [26–28]. The nitrocellulose membranes were incubated overnight with 5% nonfat dry milk in phosphate-buffer saline containing 0.1% Tween 20 (PBST). After being rinsed with PBST, the membranes were then incubated with a commercial polyclonal antibody against OAT1 (1.25 μg/mL) or against alkaline phosphatase (diluted 1:2500) for 2 h or with non-commercial rabbit polyclonal antibody against rat OAT3 (at a dilution of 1:1000) overnight. Membranes were incubated for 1 h with a peroxidase coupled goat anti-rabbit IgG (Bio-Rad) after further washing with PBST. Blots were processed for detection using commercial kits (Opti-4CN, Bio-Rad for OAT1 and ECL enhanced chemiluminescence system; Amersham for alkaline phosphatase and OAT3). An absorption test was also performed. The OAT1 peptide (1.25 μg/mL) or OAT3 peptide (0.50 mg/mL) was added to the OAT1-antibody solution or OAT3-antibody solution respectively and incubated for 2 h. Using these preabsorbed antibodies, Western blot analyses were performed as described above. A densitometric quantification of Western blot signal intensity of membranes was performed.

2.6. Immunohistochemistry microscopy

The kidneys were briefly perfused with saline, followed by perfusion with periodate–lysine–paraformaldehyde solution (0.01 M $NaIO_4$, 0.075 M lysine, 0.0375 M phosphate buffer, with 2% paraformaldehyde, pH 6.20), through an abdominal cannula. Kidneys slices were immersed in periodate–lysine–paraformaldehyde solution at 4 °C overnight. The tissue was embedded in paraffin for light microscopic immunohistochemical analysis. Paraffin sections were cut. After deparaffining, the sections were incubated with 3% H_2O_2 for 15 min (to eliminate endogenous peroxidase activity) and then with blocking serum for 15 min. The sections were then incubated with polyclonal antibodies against OAT1 or OAT3 overnight. Rabbit polyclonal antibodies were raised against a synthesized polypeptide of the carboxyl terminal of rOAT1 or of rOAT3 [29,30]. The sections were rinsed with PBST and incubated with biotinylated secondary antibody against rabbit Immunoglobulin for 1 h (biotinylated Ig Multi-Link Biogenex). After being rinsed with PBST, the sections were incubated for 30 min with horseradish peroxidase (HRP)-conjugated streptavidin solution (Streptavidin/HRP complex Multi-Link Biogenex). In order to detect HRP labeling, a peroxidase substrate solution with diaminobenzidine (0.05% diaminobenzidine in PBST with 0.05% H_2O_2) was used. The sections were counterstained with hematoxylin before being examined under a light microscopic.

2.7. Na–K-ATPase activity assay

Na–K-ATPase activity was estimated as the difference between the amounts of inorganic phosphate liberated in the absence (total ATPase) and in the presence (Mg^{+2}-ATPase) of ouabain [31]. The release of inorganic phosphate was measured according to Widnell et al. [32].

2.8. Renal excretion studies

These studies were performed as previously described [21,25,33]. Sham ($n=4$) and CRF ($n=5$) rats were anaesthetized as described. Femoral vein and artery were cannulated and a bladder catheter (3 mm i.d.) was inserted through a suprapubic incision. A priming dose of inulin (0.6 mg/kg b.w.) and PAH (30 mg/kg b.w.) in 1 mL of saline solution was administered through the venous catheter. Then, a solution containing inulin (18 g/L), PAH (6 g/L) and saline solution (9 g/L) was infused through the venous catheter employing a constant infusion pump (Pump 22; Harvard Apparatus, USA) at a rate of 1 mL/h/100 g b.w. After equilibrating for 45 min, urine was collected during two 20-min periods. Blood from the femoral artery was obtained at the midpoint of each clearance period. Arterial blood pressure was estimated throughout the experiments with a manometer inserted in the femoral artery. The glomerular filtration rate (GFR) was calculated from the clearance of inulin, in order to determine the filtered load of PAH. The excreted, secreted and filtered loads of PAH were calculated by conventional formulae for each animal. PAH concentrations in the serum and urine were determined by the method of Waugh and Beall [34] and inulin concentrations were assayed by the procedure of Roe [35]. The volume of urine was determined by gravimetry.

2.9. Pharmacokinetic studies

These studies were done similar to previously described [20,25,27]. The day of the experiments, Sham ($n=5$) and CRF ($n=6$) rats were anaesthetized with sodium thiopental (70 mg/kg b.w., i.p.). The femoral artery and the vein were both catheterized to obtain samples and to administer test compound, respectively. A single bolus of PAH (30 mg/kg b.w., aqueous solution, i.v.) was administered.

Table 1
Body weight, kidney weight, kidney/body weight ratio, systolic blood pressure (SBP), and plasma creatinine concentrations (PCr) in Sham and CRF rats

	Sham ($n=5$)	CRF ($n=6$)
Body weight (g)	494 ± 21	494 ± 28
Kidneys weight (g)	3.29 ± 0.12	2.22 ± 0.18*
Kidney/body weight ratio	0.00671 ± 0.00036	0.00446 ± 0.00019*
SBP (mm Hg)	126 ± 2	150 ± 4*
PCr (mg%)	0.94 ± 0.04	2.10 ± 0.02*

Results are expressed as mean values ± S.E.
* $P<0.05$.

Blood samples were obtained at 0–15 min range time after the administration of the PAH solution. The volume of blood samples was 50 μL. Seven blood samples were removed from each rat at different times between 0 and 15 min. An equivalent volume of isotonic saline solution was infused to restore the amount extracted in the blood samples. Samples were centrifuged at 3000 rpm for 3 min, and the extracted plasmas were frozen at −20 °C until analysis.

The plasma concentration vs. time curves for PAH, for each individual animal, were fitted with the PKCALC computer program [36]. Data were fitted to a biexponential curve. The choice of the best fit was based on the determination of coefficient values (R^2) and F test [37,38]. All fits had R^2 values >0.9. The following equation was used to describe the biexponencial concentration–time curves:

$$Cp = Ae^{-\alpha t} + Be^{-\beta t}$$

where Cp is PAH plasma concentration (mg%) at time t (min) after administration; α represents the distribution from the central compartment and β is an equilibrium constant reflecting the dynamics between k_{21} and K_{10} and the slopes of each of the adjusted curves give their values. A and B represent the initial values of the distribution and elimination components, respectively, extrapolated from the y-axis intercept. The estimate parameters (α, β, A, and B) were used to solve the first-order rate constants of transfer from the central to the peripheral compartments (k_{12} and k_{21}) and the elimination rate constant from the central compartment (K_{10}) with classical equations. The derived parameters are: area under curve (AUC), total volume of distribution (VdT), volume of the central compartment (VdC), volume of the peripheral compartment (VdP), steady-state volume of distribution (Vdss), systemic clearance (Cls), elimination half- life ($t_{1/2}$ β) were calculated according to standard procedures for compartmental analysis. Cls was calculated as Dose/AUC. The formulas for calculation of the different volume of distribution were: VdT=Dose/[Beta×AUC], VdC=Dose/A+B, VdP=VdT−VdC, Vdss=Cls×MDRT, MDRT (mean disposition residence time)=AUMC/AUC, AUMC is the area under curve for the plot of the product of concentration and time vs. the time from time zero to infinity. The concentration of PAH in plasma was measured using the method described by Waugh and Beall [34].

2.10. Materials

Chemicals were purchased from Sigma (St. Louis, MO, USA) and were analytical grade pure. Polyclonal antibody against OAT1 and the OAT1 peptide for Western blot was purchased from Alpha Diagnostic International (San Antonio, TX, USA). The polyclonal antibody against OAT1 for immunohistochemical studies and the polyclonal antibody against OAT3 and the OAT3 peptide for both Western and immunohistochemical studies were non-commercial [29,30].

2.11. Statistical analysis

Statistical analysis was performed using an unpaired t-test. When variances were not homogeneous a Welch's

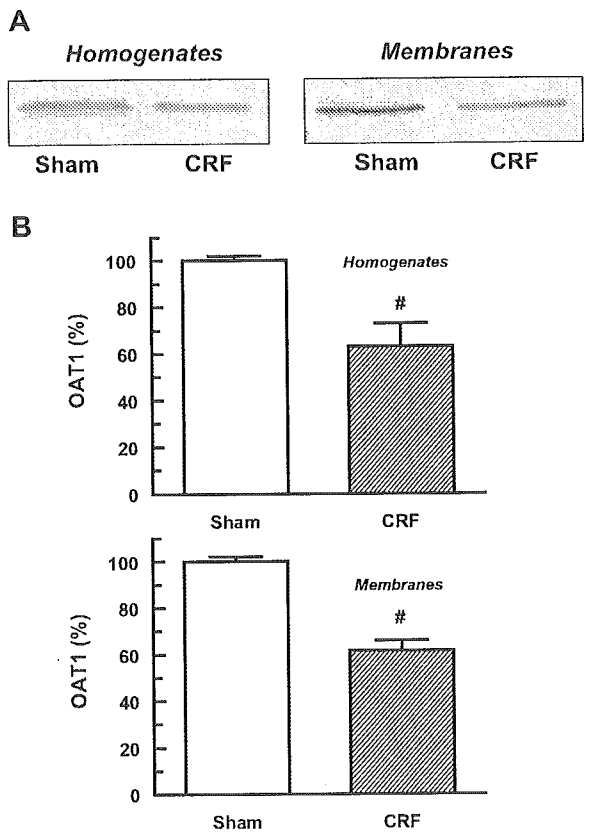

Fig. 1. (A) Renal homogenates (50 μg proteins) and basolateral membranes (50 μg proteins) from kidneys of Sham and CRF rats were separated by sodium dodecyl sulfate-polyacrylamide gel electrophoresis (8.5%) and blotted onto nitrocellulose membranes. OAT1 was identified using commercial polyclonal antibodies as described in Materials and methods. (B) Densitometric quantification of OAT1. Sham levels were set at 100%. Each column represents mean ± S.E. from experiments carried out in triplicate on four different homogenates and basolateral membrane preparations for each experimental group. $^{\#}P<0.05$.

correction was employed. P values less to 0.05 were considered significant. Values are expressed as means ± standard error (S.E.). For these analysis a GraphPad software was used.

3. Results

Body weight, kidney weight, kidney/body weight ratio, SBP and PCr are shown in Table 1. PCr levels rose to around 220% of Sham. Histological studies revealed lymphocitic infiltrate in the interstitium, a moderate dilatation of proximal tubules, decreased cellular height and tubular tiroidization (data not shown).

When kidney homogenates and basolateral plasma membranes from Sham and CRF animals were subjected to immunoblot analysis for OAT1 protein, a primary band with a size of 57 kD was detected. Fig. 1 shows a decrement of approximately 40% both in homogenates and membranes in the expression of OAT1 in CRF rats. The OAT1 protein of 57 kD disappeared when the antibody was preabsorbed to the synthetic antigen peptide (data not shown).

The immunohistochemistry using horseradish peroxidase-conjugated secondary antibody for light microscopy showed the OAT1 label associated with the basolateral plasma membrane domains of proximal tubules in Sham and CRF rats. Fig. 2 shows that OAT1 labeling was decreased in CRF rats compared with Sham ones.

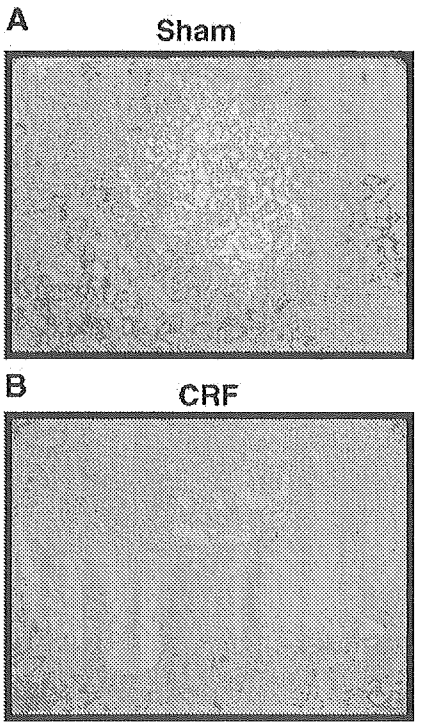

Fig. 2. Immunostaining of OAT1 in kidneys from Sham (A) and CRF rats (B). Serial sections from each rat kidney were stained using a non-commercial anti-rOAT1 antibody (crude immune serum). OAT1 labeling was seen at the basolateral domains of proximal tubule cells. In CRF rats, OAT1 labeling density was much weaker compared with that seen in kidneys from Sham-operated rats. These figures are representatives of typical samples from four rats. Magnification ×150.

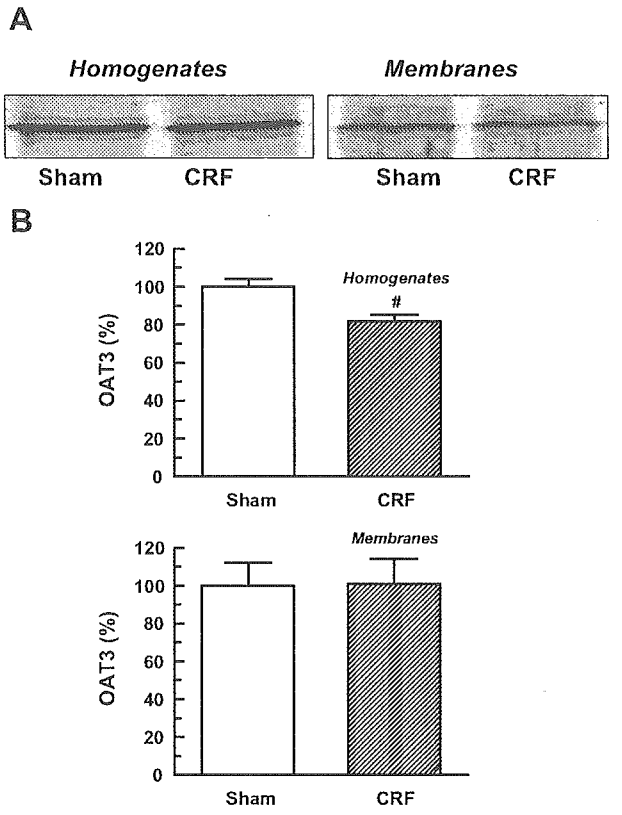

Fig. 3. (A) Renal homogenates (70 μg proteins) and basolateral membranes (70 μg proteins) from kidneys of Sham and CRF rats were separated by sodium dodecyl sulfate-polyacrylamide gel electrophoresis (8.5%) and blotted onto nitrocellulose membranes. OAT3 was identified using non-commercial polyclonal antibodies as described in Materials and methods. (B) Densitometric quantification of OAT3. Sham levels were set at 100%. Each column represents mean ± S.E. from experiments carried out in triplicate on four different homogenates and basolateral membrane preparations for each experimental group. $^{\#}P<0.05$.

Western blots of kidney homogenates and basolateral plasma membranes from Sham and CRF rats showed signals for OAT3 with a protein size of 130 kD. In Fig. 3 it can be observed that OAT3 abundance was slightly decreased in kidney homogenates from CRF rats as compared with Sham ones. The densitometry of these bands revealed a decrease in OAT3 from CRF to 82 ± 3% of sham-operated control levels. No differences were observed for OAT3 expression in basolateral plasma membranes from both experimental groups. These signals were not observed when the antibody was preabsorbed with the OAT3 peptide (data not shown).

The immunoperoxidase microscopy for OAT3 showed no appreciable differences in the staining for both Sham and CRF kidneys (data not shown).

Values of alkaline phosphatase abundance in kidney homogenates were not significantly different between Sham and CRF rats (100 ± 19%, $n=4$, vs. 103 ± 14%, $n=4$).

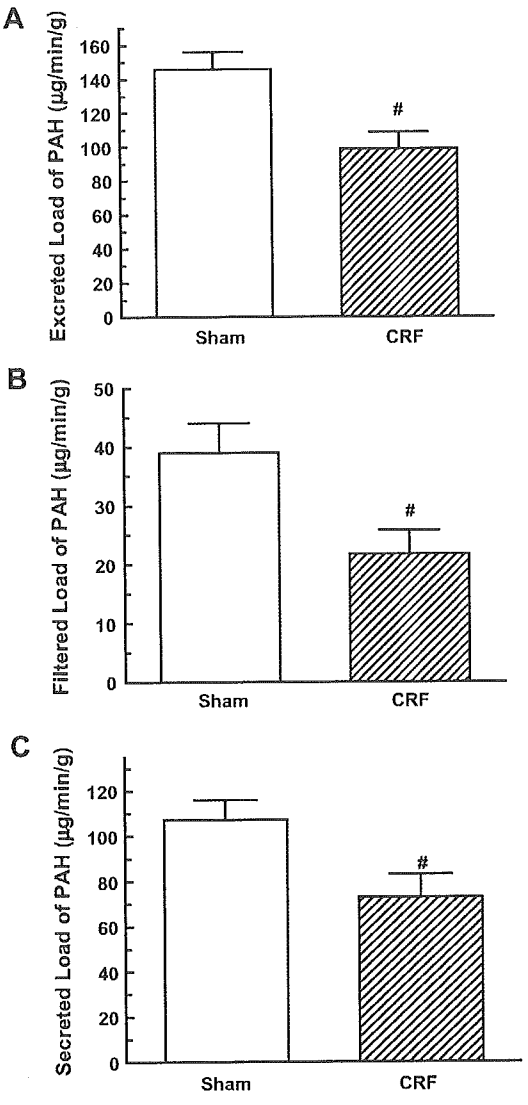

Fig. 4. Excreted (A), filtered (B) and secreted (C) loads of PAH in Sham ($n=4$) and CRF ($n=5$) rats expressed per gram of kidney weight. Results are expressed as means ± S.E. $^{\#}P<0.05$.

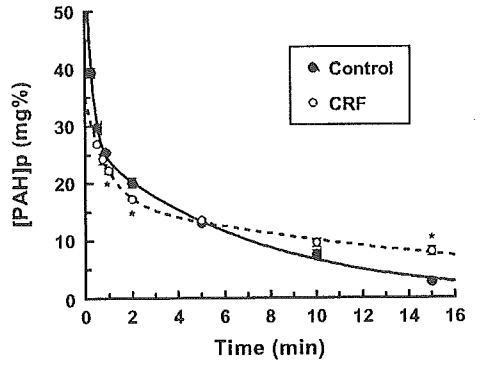

Fig. 5. Mean plasma concentration–time profiles of PAH in Sham ($n=5$) and CRF ($n=6$) rats following a single 30 mg/kg b.w., i.v. dose of PAH. Seven blood samples were taken from each animal at different times between 0 and 15 min. Results are expressed as means ± S.E. $^{*}P<0.05$. S.E. is lower than the size of the symbols for some values.

Table 2
Pharmacokinetic parameters of PAH in Sham and CRF rats after a single dose (30 mg/kg b.w., i.v.)

	Sham ($n=5$)	CRF ($n=6$)
AUC (mg × s/mL)	2.03 ± 0.07	3.80 ± 0.61*
Cls (mL/min/100 g, b.w.)	1.48 ± 0.05	0.885 ± 0.123*
K_{10} (min^{-1})	0.550 ± 0.132	0.108 ± 0.022*
$t_{1/2}$ (β) (min)	4.31 ± 0.14	9.40 ± 1.09*
VdT (mL/100 g, b.w.)	9.82 ± 0.41	16.50 ± 0.81*
VdC (mL/100 g, b.w.)	3.95 ± 1.52	8.85 ± 0.84*
VdP (mL/100 g, b.w.)	5.86 ± 1.28	7.65 ± 0.85
Vdss (mL/100 g, b.w.)	10.22 ± 0.38	15.13 ± 0.48*

Results are expressed as means ± S.E.
AUC=area under curve; Cls=systemic clearance; K_{10}=elimination constant from the central compartment; $t_{1/2}$ (β)=elimination half-life ($t_{1/2}$); VdT=total volume of distribution; VdC=volume of the central compartment; VdP=volume of the peripheral compartment; Vdss=steady-state volume of distribution.
* $P<0.05$.

The heterogeneous changes in the abundance of OAT1, OAT3 and alkaline phosphatase observed in CRF rats underline the selectivity of the response.

Na–K-ATPase activity decreased in kidney homogenates from CRF rats as compared with Sham ones (µmol Pi/h/mg protein, 9.1 ± 0.4, $n=4$, vs. 4.9 ± 0.9, $n=4$, $P<0.05$).

CRF rats showed an important decrease of GFR as compared with Sham rats (µL/min/g, 94 ± 17, $n=5$, vs. 638 ± 76, $n=4$, $P<0.05$). As shown in Fig. 4, the excreted (Fig. 4A), filtered (Fig. 4B) and secreted (Fig. 4C) loads of PAH were diminished in CRF rats. The excreted load of PAH was significantly lower in CRF group as consequence of a diminution of both filtered and secreted loads.

The pharmacokinetic studies revealed that PAH concentration decreases in the central compartment following a biexponencial function as it is shown in Fig. 5. Lower plasma concentrations of PAH in CRF group were observed at first time points. This behavior during the distribution phase might be due to the increment in the VdC observed in CRF rats. On the contrary, higher plasma concentrations of PAH in the CRF group were displayed during the elimination phase (last time points), indicating the impairment in the elimination of this organic anion. The pharmacokinetic parameters of PAH were all statistically different in CRF rats as compared with Sham ones, with the exception of VdP. Lower values of PAH systemic clearance and K_{10} in CRF rats as compared with Sham ones are shown in Table 2. In addition to the statistically significant increase in VdC, CRF rats also showed higher values of VdT and Vdss. The Vdss was used to evaluate the differences in drug distribution, since changes in VdT are also associated with changes in drug elimination [38–40].

4. Discussion

Several studies have focused in the mechanism by which renal function declines in chronic renal failure following

subtotal renal ablation but it still remains unclear. Some of them have examined the importance of glomerular changes in the initiation and progression of renal damage [1]. However, it seems that tubular damage is at least as important as glomerulosclerosis. Tubular activity and function have been little examined in CRF. Few data are available on the changes in the activity of tubular cell membranes where important transporters and energy regulators reside [5–7,16,17].

Renal impairment is closely associated with increased uremic toxicity which is characterized by accumulation of end products of protein metabolism and various hormonal peptides [41].

The dosage regimen of drugs must be modified in renal impairment because this failure has a variety of influences on pharmacokinetics and pharmacodynamics [42,43].

The mammalian renal proximal tubule plays an important function by rapidly clearing the blood of endogenous toxins and xenobiotics. In this regard, the renal organic anions secretory pathway has evolved to mediate the excretion of a wide array of negatively charged organic compounds, and PAH has become the model substrate used to functionally characterize the luminal and basolateral membrane transport mechanisms [8]. OAT1 and OAT3 represent the main basolateral polyspecific transporters for organic anions [8–11,44]. Little is known about the modulation of these transporters, especially about OAT1 and OAT3 regulatory aspects concerning the body's response to disease states. In our laboratory we have demonstrated modifications in the expression of OAT1 in kidneys from rats with different pathologies such as: arterial calcinosis [21], extrahepatic cholestasis [27] and ureteral obstruction [45].

In the present study we performed in rats with CRF, induced by means of 5/6 nephrectomy, semiquantitative immunoblotting and immunohistochemistry for OAT1 and OAT3, PAH pharmacokinetics and PAH renal excretion with the following purposes: (1) to examine whether there are changes in renal OAT1 and OAT3 expression and (2) to examine whether these changes are associated with changes in organic anions excretion.

Our data revealed that CRF rats have a lower expression of OAT1 protein in both kidney homogenates and renal basolateral membranes. These results were confirmed by immunohistochemistry. On the other hand, a slightly decrease in OAT3 expression was observed in homogenates from CRF kidneys that was not evidenced in immunohistochemistry studies. No modifications in OAT3 abundance were evidenced in renal basolateral plasma membranes from CRF group. The specificity of these alterations were also demonstrated by the lack of changes in the alkaline phosphatase protein expression in renal homogenates.

We evaluated the excretion of PAH in Sham and CRF rats. Interestingly, this parameter was diminished in CRF rats. GFR and consequently the filtered load of PAH were also lower in CRF rats as compared with Sham ones. Moreover, the secreted load of PAH was diminished in the CRF group. Therefore, the differences observed in renal excretion of PAH are accounted for variations in filtered and secreted load of this organic anion. The decrease in the renal excretion of PAH observed in CRF rats was evidenced in pharmacokinetic parameters of PAH such as K_{10} and Cls.

The medium PAH plasma concentrations reached during the renal clearance infusion studies were 314 ± 28 and 1191 ± 162 μM for Sham and CRF rats respectively. The OAT1 and OAT3 mediated uptake of PAH is saturable with apparent Michaelis constants ranging 15 to 70 μM for rat OAT1 [9,10] and 60 to 90 μM for rat OAT3 [8,11]. So, the PAH concentrations that we obtained in our "in vivo" experiments were sufficiently high above the reported Km of rat OAT1 and OAT3. The diminished secreted load of PAH measured under saturating conditions might be in part account for the lower number of OAT1 protein units observed in basolateral plasma membranes from CRF kidneys. In addition, the transport of organic anions mediated by OAT1 and OAT3 occurs by indirect coupling of the sodium gradient, and this gradient is generated by Na,K-ATPase pump. The present study shows that the Na,K-ATPase pump activity was reduced in CRF rats. In this connection, Kwon et al. [7] have reported that there is significant decrease in total kidney levels of Na,K-ATPase in rats with CRF. Moreover, Maxild et al. [46] have demonstrated that the inhibition of aerobic accumulation of PAH by ouabain in cortex slices of rabbit kidney is related to a decrease in Na,K-ATPase activity.

Contrasting with OAT1 down regulation, MRP2 upregulation in CRF rats has been described by Laouari et al. [16]. Therefore, the protein expression of the luminal (MRP2) and basolateral (OAT1) PAH transporters are differently modified in CRF. As highly accumulated anionic drugs may cause further deterioration of renal failure, the molecular mechanism(s) involved in the differential regulation of MRP2 and OAT1 expression should be elucidated to prevent drug-induced toxicity under CRF. Tubular secretion is a vectorial transcelular transport system consisting of basolateral entry into the epithelial cells and efflux across the brush border membranes. Defects in either of these two processes should influence the tubular secretion of ionic drugs. In the present study, the tubular secretion of PAH was markedly reduced, corroborating the concept that the limiting step for the urinary excretion of PAH is the tubular secretion step across the basolateral membranes.

It is also important to mention that there might be other factors involved in the reduced PAH renal excretion in CRF such as the reduction in renal blood flow [1] that limits the delivery of the drug to the OAT1 and the competition for peritubular uptake [8,47] and for luminal secretion [48] with other organic anions that include urate

[9] that accumulate in uremia. Metabolic acidosis, that is another characteristic feature of CRF, depolarizes the membrane potential of proximal tubule cells [49] decreasing consequently organic anions secretion. The increased VdT as consequence of the increment in VdC that we observed in CRF rats might also contribute to decrease renal PAH delivery. The increase in this VdC might be due to the fact that animals with CRF have a 10 to 30% increment in extracellular and blood volume [50].

CRF is well known to be associated with elevated serum parathyroid hormone (PTH) levels and changes in mineral ion homeostasis including secondary hyperparathyrodism [1]. Nagai and co-workers [51] have showed an inhibition of basolateral uptake and secretion of organic anions in opossum kidney (OK) cells by parathyroid hormone via a staurosporine sensitive mechanism. The inhibition of basolateral OAT1 by stimulation of protein kinase C (PKC) has been reported in isolated tubules of killifish [52]. Recently, You and co-workers [53] have showed that PKC inhibits murine OAT1 without direct phosphorylation of the transport protein itself. Since PTH is a potent inhibitor of organic anion transport by PKC we speculate that the decreased density and kidney levels of OAT1 in rats with CRF in the present study may be at least partly attributed to the increased levels of serum PTH.

OAT1 also transports diuretics [47]. Its reduced expression might also explain the manifest diuretic resistance in patients with CRF [54]. It is well known that diuretics achieve their site of action after being secreted in the tubular lumen by means of the organic anions transport system. These data would throw new light on mechanisms that contribute to diuretic resistance in models or patients with CRF.

In conclusion, the goal of this study was to evaluate for the first time OAT1 and OAT3 expression in severe CRF. This study demonstrates the functional and molecular alterations of the urinary excretion mechanisms of organic anions in 5/6 nephrectomized rats. The reduction in the protein expression of OAT1 (approximately 40%) or in the activity of Na,K-ATPase pump (approximately 45%) or both would be, at least in part, associated with the organic anions secretion impairment in CRF, which substantially alters the renal capacity for eliminating these compounds and accounts for some accumulated uremic toxins found in CRF.

Acknowledgements

Support for this study was provided by FONCYT (PICT 05-06160). The authors thank to Miss Alcira Gallego (ININCA, Facultad de Medicina, UBA, CONICET), Lic. Graciela Ottaviano (ININCA, CONICET) and Mrs. Alejandra Martínez (Facultad de Ciencias Bioquímicas y Farmacéuticas, UNR) for their technical assistance. AMT received a Travel Grant from CONICET/JSPS (Japan Society for the Promotion of Science).

References

[1] M. Lasky, N.A. Kurtzman, S. Sabatini, Chronic renal failure, in: D.W. Seldin, G. Giebisch (Eds.), The Kidney Physiology and Pathophysiology, Lippincott Williams & Wilkins, Philadelphia, USA, 2000, pp. 2375–2410.

[2] B.F. Palmer, The renal tubule in the progression of chronic renal failure, J. Investig. Med. 45 (1997) 346–361.

[3] L.G. Fine, W. Trizna, J.J. Bourgoigne, Functional profile of the isolated uremic nephron: role of compensatory hypertrophy in the control of fluid reabsorption by the proximal straight tubule, J. Clin. Invest. 61 (1978) 1508–1518.

[4] D.C.H. Harris, L. Chan, R.W. Schrier, Remnant kidney hypermetabolism and progression of chronic renal failure, Am. J. Physiol. 254 (1988) F267–F276.

[5] D. Laouari, G. Friedlander, M. Burtin, C. Silve, M. Dechaux, M. Garabedian, C. Kleinknecht, Subtotal nephrectomy alters tubular function: effect of phosphorus restriction, Kidney Int. 52 (1997) 1550–1560.

[6] T.H. Kwon, J. Frokiaer, P. Fernandez-Llama, A.B. Maunsbach, M.A. Knepper, S. Nielsen, Altered expression of Na transporters NHE-3, NaPi-II, Na–K-ATPase, BSC-1 and TSC in CRF rats, Am. J. Physiol. 277 (1999) F257–F270.

[7] T.H. Kwon, J. Frokiaer, M.A. Knepper, S. Nielsen, Reduced AQP1,-2, and -3 levels in kidneys of rats with CRF induced by surgical reduction in renal mass, Am. J. Physiol. 275 (1998) F724–F741.

[8] S.H. Wright, W.H. Dantzler, Molecular and cellular physiology of renal organic cation and anion transport, Physiol. Rev. 84 (2004) 987–1049.

[9] T. Sekine, N. Watanabe, M. Hosoyamada, Y. Kanai, H. Endou, Expression cloning and characterization of a novel multispecific organic anion transporter, J. Biol. Chem. 272 (1997) 18526–18529.

[10] D.H. Sweet, N.A. Wolff, J.B. Pritchard, Expression cloning and characterization of ROAT1: the basolateral organic anion transporter in rat kidney, J. Biol. Chem. 272 (1997) 30088–30095.

[11] S.H. Cha, T. Sekine, J.-I. Fukushima, Y. Kanai, Y. Kobayashi, T. Goya, H. Endou, Identification and characterization of human organic anion transporter 3 expressing predominantly in the kidney, Mol. Pharmacol. 59 (2001) 1277–1286.

[12] R. Van Aubel, J.G. Peters, R. Masereeuw, C.H. Van Os, F.G.M. Russel, Multidrug resistance protein Mrp2 mediates ATP-dependent transport of classical renal organic anion *p*-aminohippurate, Am. J. Physiol. 279 (2000) F713–F717.

[13] I. Leier, J. Hummel-Eisenbeiss, Y. Cui, D. Keppler, ATP-dependent *para*-aminohippurate transport by apical multidrug resistance protein MRP2, Kidney Int. 57 (2000) 1636–1642.

[14] P.H. Smeets, R.A. van Aubel, A.C. Wouterse, J.J. van den Heuvel, F.G. Russel, Contribution of multidrug resistance protein 2 (MRP2/ABCC2) to the renal excretion of *p*-aminohippurate (PAH) and identification of MRP4 (ABCC4) as a novel PAH transporter, J. Am. Soc. Nephrol. 15 (2004) 2828–2835.

[15] R. van Aubel, R. Masereeuw, F.G.M. Russel, Molecular pharmacology of organic anion transporters, Am. J. Physiol. 279 (2000) F216–F232.

[16] D. Laouari, R. Yang, C. Veau, I. Blanke, G. Friedlander, Two apical multidrug transporters, P-gp and MRP2, are differently altered in chronic renal failure, Am. J. Physiol. 280 (2001) F636–F645.

[17] A. Takeuchi, S. Masuda, H. Saito, T. Doi, K. Inui, Role of kidney-specific organic anion transporters in the urinary excretion of methotrexate, Kidney Int. 60 (2001) 1058–1068.

[18] A.B. Morrison, Experimentally induced chronic renal insufficiency in the rat, Lab. Invest. 11 (1962) 321–332.

[19] M. MacLaughlin, A.J. Monserrat, A. Muller, M. Matoso, C. Amorena, Role of kinins in the renoprotective effect of angiotensin-converting enzyme inhibitors in experimental chronic renal failure, Kidney Blood Press. Res. 21 (1998) 329–334.

[20] N.B. Quaglia, C.G. Hofer, A.M. Torres, Pharmacokinetics of organic anions in rats with arterial calcinosis, Clin. Exp. Pharmacol. Physiol. 29 (2002) 48–52.
[21] N.B. Quaglia, A. Brandoni, A. Ferri, A.M. Torres, Early manifestation of nephropathy in rats with arterial calcinosis, Ren. Fail. 25 (2003) 355–366.
[22] K. Thomsen, The effect of sodium chloride on kidney function in rats with lithium intoxication, Acta Pharm. Toxicol. (Copenh) 33 (1973) 92–102.
[23] J.J. Sedmak, S.E. Grossberg, A rapid, sensitive and versatile assay for protein using Coomassie Brilliant Blue G250, Anal. Biochem. 79 (1977) 544–552.
[24] R.E. Jensen, W.O. Berndt, Epinephrine and norepinephrine enhance *p*-aminohippurate transport into basolateral membrane vesicles, J. Pharmacol. Exp. Ther. 244 (1988) 543–549.
[25] J.A. Cerrutti, N.B. Quaglia, A.M. Torres, Characterization of the mechanisms involved in the gender differences in *p*-aminohippurate renal elimination in rats, Can. J. Physiol. Pharm. 79 (2001) 805–813.
[26] J.A. Cerrutti, A. Brandoni, N.B. Quaglia, A.M. Torres, Sex differences in *p*-aminohippuric acid transport in rat kidney: role of membrane fluidity and expression of OAT1, Mol. Cell. Biochem. 233 (2002) 175–179.
[27] A. Brandoni, N.B. Quaglia, A.M. Torres, Compensation increase in organic anion excretion in rats with acute biliary obstruction: role of the renal organic anion transporter 1, Pharmacology 68 (2003) 57–63.
[28] V. Shah, S. Cao, H. Hendrickson, J. Yao, Z.S. Katusic, Regulation of hepatic eNOS by caveolin and calmodulin after bile duct ligation in rats, Am. J. Physiol. 280 (2001) G1209–G1216.
[29] A. Tojo, T. Sekine, N. Nakajima, M. Hosoyamada, Y. Kanai, K. Kimura, H. Endou, Immunohistochemical localization of multispecific renal organic anion transporter 1 in rat kidney, J. Am. Soc. Nephrol. 10 (1999) 464–471.
[30] R. Kojima, T. Sekine, M. Kawachi, S.H. Cha, Y. Suzuki, H. Endou, Immunolocalization of multispecific organic anion transporters, OAT1, OAT2, and OAT3, in rat kidney, J. Am. Soc. Nephrol. 13 (2002) 848–857.
[31] W. Schoner, C. Von Ilberg, R. Kramer, W. Seubert, On the mechanism of Na+ and K+ stimulation hydrolysis of adenosine triphosphate, Eur. J. Biochem. 1 (1967) 334–343.
[32] C.B. Widnell, Purification of rat liver 5′ nucleotidase as a complex with sphingomyelin, Methods Enzymol. 32 (1974) 368–374.
[33] A. Brandoni, S.R. Villar, A.M. Torres, Gender-related differences in the pharmacodynamics of furosemide in rats, Pharmacology 70 (2004) 107–112.
[34] W.H. Waugh, P.T. Beall, Simplified measurement of PAH and other arylamines in plasma and urine, Kidney Int. 5 (1974) 429–432.
[35] H.H. Roe, A photometric method for determination of inulin in plasma and urine, J. Biol. Chem. 178 (1949) 839–844.
[36] R. Shumaker, PKCALC: a basic interactive computer program for statistical and pharmacokinetic analysis of data, Drug Metab. Rev. 17 (1986) 331–348.
[37] H. Motulsky, Using nonlinear regression to fit curves, in: H. Motulsky (Ed.), Intuitive Biostatistics, Oxford University Press, New York, 1995, pp. 227–283.
[38] A. Velasco, Absorción, distribución, eliminación y biotransformación de los fármacos, in: Velasco, et al., (Eds.), Velazquez Farmacología, 16 edition, MacGraw-Hill Interamericana, Madrid, España, 1993.
[39] J. Molpeceres, M. Chacon, L. Berges, J.L. Pedraz, M. Guzmán, M.R. Aberturas, Age and sex dependent pharmacokinetics of cyclosporine in the rat after a single intravenous dose, Int. J. Pharm. 174 (1998) 9–18.
[40] M. Gibaldi, D. Perrier, Pharmacokinetics, Ed. M. Dekker, New York, USA, 1982.
[41] D. Powell, J. Bergstrom, R. Dzurik, P. Gulyassy, D. Lockwood, L. Phillips, Toxins and inhibitors in chronic renal failure, Am. J. Kidney Dis. 7 (1986) 292–299.
[42] T.P. Gibson, Influence of renal disease on pharmacokinetics, in: W.E. Evans, J.S. Schentag, W.J. Jusko (Eds.), Applied Pharmacokinetics, Applied Therapeutics, Inc, Spokane, 1986, pp. 698–719.
[43] P. Sweny, K. Farrington, J.F. Moorhead, Prescribing of drugs in renal failure, The Kidney and Its Disorders, Blackwell Scientific Publications, Oxford, 1989, pp. 698–719.
[44] T. Sekine, K. Watanabe, M. Hosoyamada, N. Kanai, H. Endou, A novel multispecific organic anion transporter (PAH transporter): its structure and functional characteristics, Nova Acta Leopold. 306 (1998) 119–126.
[45] S.R. Villar, A. Brandoni, N.B. Quaglia, A.M. Torres, Renal elimination of organic anions in rats with bilateral ureteral obstruction, Biochim. Biophys. Acta 1688 (2004) 204–209.
[46] J. Maxild, J.V. Moller, I. Sheikh, Involvement of Na–K-ATPase in *p*-aminohippurate transport by rabbit kidney tissue, J. Physiol. 315 (1981) 189–201.
[47] Y. Uwai, H. Saito, Y. Hashimoto, K.I. Inui, Interaction and transport of thiazide diuretics, loop diuretics, and acetazolamide via rat renal organic anion transporter r OAT1, J. Pharmacol. Exp. Ther. 295 (2000) 261–265.
[48] W. Krick, N.A. Wolff, G. Burckhardt, Voltage-driven *p*-aminohippurate, chloride, and urate transport in porcine renal brush-border membrane vesicles, Pflügers Arch. 441 (2000) 125–132.
[49] D. Cemerikic, C.S. Wilcox, G. Giebisch, Intracellular potential and K activity in rat kidney proximal tubular cells in acidosis and K depletion, J. Membr. Biol. 69 (1982) 159–165.
[50] R.S. Mathias, H.T. Nguyen, M. Zhang, A.A. Portale, Reduced expression of the renal calcium-sensing receptor in rats with experimental chronic renal insufficiency, J. Am. Soc. Nephrol. 9 (1998) 2067–2074.
[51] J. Nagai, I. Yano, Y. Hashimoto, M. Takano, K. Inui, Inhibition of PAH transport by parathyroid hormone in OK cells: involvement of protein kinase C pathway, Am. J. Physiol. 273 (1997) F674–F679.
[52] D.S. Miller, Protein kinase C regulation of organic anion transport in renal proximal tubule, Am. J. Physiol. 274 (1998) F156–F164.
[53] G. You, K. Kuze, R.A. Kohanski, K. Amsler, S. Henderson, Regulation of mOAT-mediated organic anion transport by okadaic acid and protein kinase C in LLC-PK1 cells, J. Biol. Chem. 275 (2000) 10278–10284.
[54] C.S. Wilcox, New insights into diuretic use in patients with chronic renal disease, J. Am. Soc. Nephrol. 13 (2002) 798–805.

Pharmaceutical Research, Vol. 22, No. 6, June 2005 (© 2005)
DOI: 10.1007/s11095-005-4580-5

Research Paper

Interactions of Stevioside and Steviol with Renal Organic Anion Transporters in S2 Cells and Mouse Renal Cortical Slices

Chutima Srimaroeng,[1,2] Promsuk Jutabha,[3] John B. Pritchard,[2] Hitoshi Endou,[3] and Varanuj Chatsudthipong[1,4]

Received January 8, 2005; accepted February 17, 2005

Purpose. Our previous studies have shown that both stevioside and steviol inhibited transepithelial transport of *para*-aminohippurate (PAH) in isolated rabbit renal proximal tubules by interfering with organic anion transport system. The current study examined the direct interactions of stevioside and steviol with specific organic anion transporters.
Methods. S2 cells expressing human organic anion transporters (hOAT1, hOAT2, hOAT3, and hOAT4) and an intact renal epithelium were used to determine the inhibitory effect of stevioside and steviol on organic anion transport.
Results. Stevioside at 0.5–1 mM showed no interaction with any OAT. In contrast, steviol markedly inhibited substrate uptake in all S2hOAT cells. Steviol had low IC_{50} values for hOAT1 (11.4 μM) and hOAT3 (36.5 μM) similar to that of probenecid, whereas IC_{50} values for hOAT2 (1000 μM) and hOAT4 (285 μM) were much higher. Results obtained in mouse renal cortical slices were very similar; that is, stevioside was without inhibitory effect and steviol was a potent inhibitor of PAH and estrone sulfate (ES) transport.
Conclusions. Stevioside has no interaction with human or mouse OATs. In contrast, steviol interacts directly with human OATs, in particular, hOAT1 and hOAT3, with a potency approximating probenecid, suggesting that the inhibition of OAT-mediated transport by steviol could alter renal drug clearance.

KEY WORDS: organic anion; organic anion transporter; renal cortical slices; steviol; stevioside.

INTRODUCTION

Stevioside is the major sweet component isolated from the leaves of *Stevia rebaudiana*. It is about 300 times sweeter than sucrose, but it is noncaloric (1). Therefore, it has become popular as a sweetener in Asia and South America and has been used as a dietary supplement in the United States (2). Stevioside can be degraded to its major metabolite, steviol, by intestinal bacterial microflora from various species including man (3–5). The chemical structures of stevioside and steviol are shown in Fig. 1. Stevioside has been shown to have therapeutic value as an antihypertensive or antihyperglycemic agent (6–10). The available data indicate that stevioside is nontoxic, nonmutagenic and noncarcinogenic in various mammalian species (11,12). In contrast, its aglycone metabolite, steviol, has been reported to be mutagenic in *Salmonella typhimurium* TM677 (13). Likewise, at doses ~6 g/kg BW, steviol was lethal to the hamster, and its LD_{50} value was ~15 g/kg BW in rats and mice (12). Thus, questions remain concerning the toxicity of stevioside and steviol that should be addressed prior to their widespread commercial use as food additives or drugs.

In particular, the renal handling of these agents is critical, as it determines the ease with which they are cleared from the body, or conversely the potential for their accumulation upon chronic consumption. Previous studies have shown that stevioside and steviol inhibited PAH uptake in rat renal cortical slices (14), suggesting that one or both compounds may be handled by the organic anion secretory system of the kidney. Indeed, our own earlier study indicated that a pharmacological concentration (0.7 mM) of stevioside inhibited transepithelial transport of PAH without changes in Na^+/K^+-ATPase activity or cellular ATP content in isolated S2 segments of rabbit renal proximal tubule (15). We also found that steviol inhibited transepithelial transport of PAH at the basolateral entry step by competitive inhibition, suggesting that steviol binds to basolateral organic anion transporter (OATs) (16). However, this *in vitro* study did not permit the clear differentiation between the interactions of stevioside and steviol with the specific organic anion transporters. Currently, several organic anion transporter isoforms have been cloned and characterized. In humans,

[1] Department of Physiology, Faculty of Science, Mahidol University, Bangkok, Thailand.
[2] Laboratory of Pharmacology and Chemistry, NIEHS, National Institutes of Health, Research Triangle Park, North Carolina, USA.
[3] Department of Pharmacology and Toxicology, Kyorin University School of Medicine, Tokyo, Japan.
[4] To whom correspondence should be addressed. (e-mail: scvcs@mahidol.ac.th)

ABBREVIATIONS: D-PBS, Dulbecco's modified phosphate-buffered saline; ES, estrone sulfate; hOAT, human organic anion transporter; PAH, *para*-aminohippurate; $PGF_{2\alpha}$, prostaglandin; TEA, tetraethylammonium.

0724-8741/05/0600-0858/0

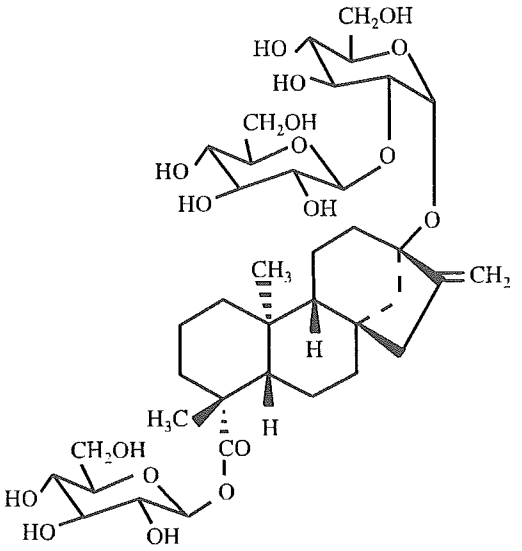

Stevioside ($C_{38}H_{60}O_{18}$)

MW 804.9

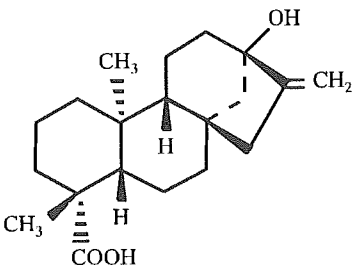

Steviol ($C_{20}H_{30}O_3$)

MW 318.4

Fig. 1. The chemical structures of stevioside and steviol.

OAT1, OAT2, and OAT3 are expressed at the basolateral membrane (17–19), whereas OAT4 is expressed at the apical membrane of the proximal tubule (20,21). These transporters play important roles for the net elimination of various organic anion compounds including therapeutic drugs. The inhibition of basolateral OATs could also reduce clearance of those therapeutic drugs transported by the OATs, potentially leading to altered therapeutic efficacy or even increased toxic side-effects of these drugs. For example, it was shown recently that methotrexate transport via hOAT1, hOAT3, and hOAT4 was inhibited by probenecid, penicillin G, and nonsteroidal inflammatory drugs (NSAIDs) (22). Therefore, these human OATs are potential sites of interactions between stevioside and steviol with anionic drugs as well.

The purpose of this study was to investigate the direct interactions of stevioside and steviol with specific renal organic anion transporters. Both S2 cells expressing specific organic anion transporters, hOAT1, hOAT2, hOAT3, hOAT4, and mouse renal cortical slices were used to determine the inhibitory effects of stevioside and steviol on organic anion transport.

MATERIALS AND METHODS

Chemicals

[^{3}H]-PAH (1480 GBq/mmol) was purchased from American Radiolabeled Chemicals, Inc. (St. Louis, MO, USA), and [^{14}C]-PAH (1.50 GBq/mmol), [^{3}H]-$PGF_{2\alpha}$ (6808 GBq/mmol), and [^{3}H]-ES (1861 GBq/mmol) were purchased from New England Nuclear Corp (Boston, MA, USA). Unlabeled PAH and ES, probenecid, α-ketoglutarate, glutarate, furosemide, bumetanide, indomethacin, cimetidine, methotrexate, tetraethylammonium (TEA), transferrin, and SRB were purchased from Sigma (St. Louis, MO, USA). Epidermal growth factor was purchased from Wakunaga (Hiroshima, Japan). Insulin was purchased from Shimizu (Shizuoka, Japan), RITC 80-7 culture medium was purchased from Iwaki Co. (Tokyo, Japan). Stevioside (≥98% purity) and steviol (≥98% purity) were kindly provided by Dr. Chaivat Toskulkao (Department of Physiology, Faculty of Science, Mahidol University, Thailand) (12). The purity of both compounds was analyzed by high-performance liquid chromatography (HPLC) (unpublished data). All other chemicals and reagents used were analytical grade and obtained from commercial sources.

Cell Cultures

Cells from the S2 segment of the proximal tubule transfected with human organic anion transporters hOAT1, hOAT2, hOAT3, and hOAT4 (designated as S2hOAT1, S2hOAT2, S2hOAT3, and S2hOAT4) used in this work were established previously (22,23). They were derived from transgenic mice harboring the temperature-sensitive simian virus 40 large T-antigen genes. Briefly, the OAT-transfected cell lines were obtained by transfection of S2 cells with pcDNA 3.1 containing each of the human OATs 1–4 coupled with pSV2neo, a neomycin resistance gene, using TfX-50 according to the manufacturer's instructions (Promega, Madison, WI, USA). S2 cells transfected with pcDNA 3.1 lacking an insert and pSV2neo were designated as S2mock and used as control group. These cells were grown in RITC 80-7 medium containing 5% fetal bovine serum, 10 mg/ml transferrin, 0.08 U/ml insulin, 10 ng/ml recombinant epidermal growth factor, and 400 mg/ml geneticin in a humidified incubator under 5% CO_2/95% air at 33°C, a permissive temperature for these cell lines. The cells were subcultured in the medium containing 0.05% trypsin-EDTA solution (in mM: 137 NaCl, 5.4 KCl, 5.5 glucose, 4 $NaHCO_3$, 0.5 EDTA, and 5 HEPES, pH 7.2).

Organic Anion Uptake

The transfected S2 cell lines were seeded in 24-well tissue culture plates at a cell density of 1×10^5 cells/well. After culturing for 2 days, uptake experiments were performed at 37°C. Based on the literature, the following substrates were used to determine transport by the human-transfected S2 cell lines: [^{14}C]-PAH for hOAT1 (17), [^{3}H]-prostaglandin $F_{2\alpha}$($PGF_{2\alpha}$) for hOAT2 (23), and [^{3}H]-estrone sulfate (ES) for hOAT3 and hOAT4 (18,20). For transport measurement, the cells were first washed three times with incubation

medium, Dulbecco's modified phosphate-buffered saline (D-PBS) (in mM: 137 NaCl, 3 KCl, 8 $NaHPO_4$, 1 KH_2PO_4, 1 $CaCl_2$, 0.5 $MgCl_2$, and 5.6 D-glucose, pH 7.4), and preincubated in the same solution for 10 min. The cells were then incubated for 30 s for hOAT2 and 2 min for hOAT1, hOAT3, and hOAT4 (approximates initial rate of uptake for each substrate via its transporters) (data not shown) in the D-PBS solution containing specific substrates, 5 μM [^{14}C]-PAH for hOAT1, 50 nM [^{3}H]-$PGF_{2\alpha}$ for hOAT2, or 50 nM [^{3}H]-ES for hOAT3 and hOAT4 in the absence or presence of stevioside and steviol. Uptake was stopped by the addition of ice-cold D-PBS solution, and the cells were washed three times with the same solution. The cells in each well were lysed with 0.5 ml of 0.1 N NaOH, and the radioactivity was measured by liquid scintillation spectrometry (1214 Rackbeta, LKB Wallac, Sweden).

Kinetic Analysis of Steviol Inhibition of PAH

S2 cells expressing hOAT1 were preincubated in D-PBS solution at 37°C for 10 min as described above. They were then incubated in D-PBS containing [^{14}C]-PAH at concentrations from 10 to 600 μM in the absence and presence of steviol for 2 min. The inhibitory constants (IC_{50}) were calculated from sigmoidal dose-response analysis using GraphPad Prism version 4.00 for windows (GraphPad Software, San Diego, CA, USA). The data were plotted as a Lineweaver–Burk plot (1/[PAH] *vs.* 1/[PAH] uptake) and the K_m (Michaelis–Menten constant) was estimated from the *x*-axis intercept. The maximal rate of PAH uptake (V_{max}) mediated by hOAT1 was estimated from the *y*-axis intercept. The K_i of steviol for PAH transport was calculated to determine the affinity of steviol for the transporter as shown in the following equation for competitive inhibition (24):

$$K_i = \frac{IC_{50}}{\left(\frac{1 + \text{concentration of steviol}}{K_m}\right)}$$

Cell Viability

Cell viability was determined using a modified colorimetric assay with sulforhodamine B (SRB) as described previously (25). This assay measures the cellular protein content of adherent cultured cells. Briefly, the cells were seeded into 96-well microtiter plate at a cell density of 1.5×10^4 cells/well and incubated at 33°C in the medium containing various concentrations of stevioside and steviol for 3 days. After incubation, the medium containing nonviable cells and serum protein was removed, and the monolayer cells were fixed with cold 20% (w/v) trichloroacetic acid (TCA) for 30 min at 4°C. They were then washed five times with distilled water and air-dried. Subsequently, the cells were stained for 30 min at room temperature by 0.4% (w/v) SRB dissolved in 1% acetic acid. At the end of staining period, SRB was removed and quickly rinsed five times with 1% acetic acid. The cellular protein contents were extracted with 10 mM Tris–base [tris (hydroxymethyl) aminomethane] and the absorbance at 515 nm was measured using a computer-interfaced, 96-well microtiter plate reader (EL 312, Bio-Kinetics reader, Bio-Tek Instrument Inc, Finland).

Animals

Adult male C57BL/6 mice raised at the National Institute of Environmental Health Sciences, NIEHS, (Research Triangle Park, NC, USA) were used in renal cortical slice experiments. All animal procedures were approved by the NIEHS Animal Care and Use Committee.

Renal Slice Preparation and Uptake Study

Tissue slices were prepared according to published methods (26). Briefly, animals were euthanized by CO_2 inhalation and decapitated. Renal cortical slices (≤0.5 mm; 5–20 mg, wet weight) were cut with a Stadie-Riggs microtome and maintained in ice-cold oxygenated modified Cross and Taggart buffer (in mM: 95 NaCl, 80 mannitol, 5 KCl, 0.74 $CaCl_2$, and 9.5 Na_2HPO_4, pH 7.4). The slices were incubated in 1 ml of buffer containing either 10 μM [^{3}H]-PAH or 100 nM [^{3}H]-ES in the absence and presence of stevioside, steviol, and various compounds for 60 min. Uptake was stopped by the addition of ice-cold buffer. Slices were washed, blotted, weighed, dissolved in 1 ml of 1 N NaOH, and neutralized with 1 ml of 1 N HCl. Nine milliliters of scintillation fluid (Ecolume, ICN, Irvine, CA, USA) was added, and radioactivity was measured using a Tri-Carb 2900TR Liquid Scintillation Analyzer (Packard, Meriden, CT, USA). The uptake of PAH and ES were calculated as tissue to medium (T/M) ratio (i.e., dpm/mg of tissue divided by dpm/μl of medium) and then expressed as a mean percentage of the control.

Statistical Analysis

Data were expressed as means ± SE. Statistical differences were assessed using one-way analysis of variance. Differences were considered to be significant when $p < 0.05$, $p < 0.01$, $p < 0.001$ *vs.* control.

RESULTS

Interactions of Stevioside and Steviol with Specific Organic Anion Transporters

To determine the direct interactions of stevioside and steviol with organic anion transporters, *cis*-inhibition studies were conducted in S2hOAT1, S2hOAT2, S2hOAT3, and S2hOAT4 cells. Steviol markedly inhibited PAH uptake in S2hOAT1, $PGF_{2\alpha}$ uptake in S2hOAT2, and ES uptake in S2hOAT3 and S2hOAT4 cells. The calculated IC_{50} of steviol were 11.4 ± 0.3, 1000 ± 31, 36.5 ± 2.6, and 285 ± 1 μM for S2hOAT1, S2hOAT2, S2hOAT3, and S2hOAT4, respectively. In contrast, the parent compound, stevioside, at concentrations up to 1 mM did not affect substrate uptake in any of the OAT-expressing cell lines (see below). Because steviol showed higher affinity for hOAT1 and hOAT3 than for hOAT2 and hOAT4, we, therefore, focused our further study on the effects of stevioside and steviol on PAH transport by S2hOAT1 cells and ES transport by S2hOAT3 cells.

As shown in Fig. 2A, stevioside had no inhibitory effect on PAH uptake in S2hOAT1 cells at all concentrations tested; whereas 10 μM to 1 mM steviol very effectively

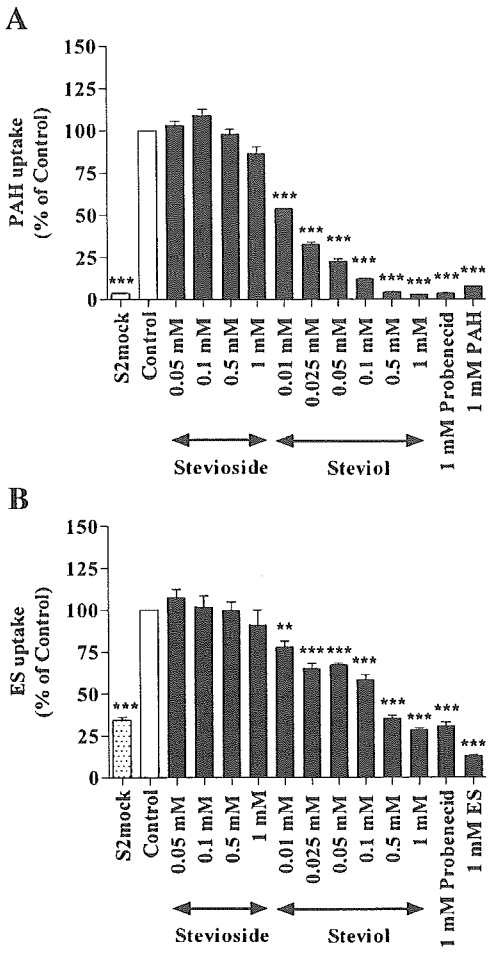

Fig. 2. The effects of stevioside and steviol on hOAT1 (A) and hOAT3 (B) mediated [^{14}C]-PAH and [^{3}H]-ES uptake in S2 cells. The uptake measurements were carried out in the presence of stevioside and steviol at various concentrations for 2 min in D-PBS containing either 5 μM of [^{14}C]-PAH for hOAT1 or 50 nM of [^{3}H]-ES for hOAT3. Unlabeled PAH, unlabeled ES, and probenecid were used to block the PAH and ES uptake in comparison with stevioside and steviol. The uptake is expressed as a mean percentage of control (mean ± SE) from three separate experiments. Mean control PAH and ES uptake were 57.2 ± 4.2 and 0.3 ± 0.1 pmol mg protein^{-1} min^{-1}, respectively. *p < 0.05, **p < 0.01, ***p < 0.001 *vs.* control.

inhibited hOAT1-mediated PAH transport in a dose-dependent manner. Stevioside at low concentrations slightly enhanced ES uptake mediated by S2hOAT3 cells, but this effect was not significant. Steviol significantly inhibited ES uptake in a dose-dependent manner at the concentrations from 10 μM to 1 mM (Fig. 2B). Importantly, 1 mM steviol inhibited PAH and ES uptake very nearly as effectively as probenecid in both S2hOAT1 and S2hOAT3 cells. For relative comparison, the IC_{50} of steviol and probenecid were 11.4 ± 0.3 and 11.9 ± 1.4 μM for S2hOAT1cells and 36.5 ± 2.6 and 4.7 ± 1.0 μM for S2hOAT3 cells, respectively.

Inhibitory Effectiveness of Steviol

The inhibitory effects of several organic compounds (100 μM) including stevioside and steviol against PAH uptake via S2hOAT1 cells were assessed (Fig. 3A). PAH uptake by S2hOAT1 cells was markedly reduced by cimetidine, unlabeled ES and PAH, bumetanide, furosemide, probenecid, steviol, and indomethacin, whereas several compounds including stevioside, TEA, and methotrexate had no effect on PAH uptake. The inhibitory effectiveness of various organic compounds on ES uptake by S2hOAT3 cells was also investigated (Fig. 3B). Stevioside 100 μM had no effect on ES uptake mediated by S2hOAT3 cells, whereas methotrexate, furosemide, TEA, unlabeled PAH, steviol, bumetanide, cimetidine, probenecid, unlabeled ES, and indomethacin all significantly inhibited ES uptake.

Kinetic Analysis of Steviol Inhibition

As shown in Fig. 4, the kinetic of PAH uptake by S2hOAT1 cells was determined in the absence and presence of 20 μM of steviol. Based on the mean values plotted in Fig. 4, the estimated K_m for PAH uptake in the presence of 20 μM of steviol was 267 μM, five times the control K_m of 52 μM. The V_{max} for PAH uptake in the presence of steviol was not markedly different from control (952 *vs.* 1030 pmol

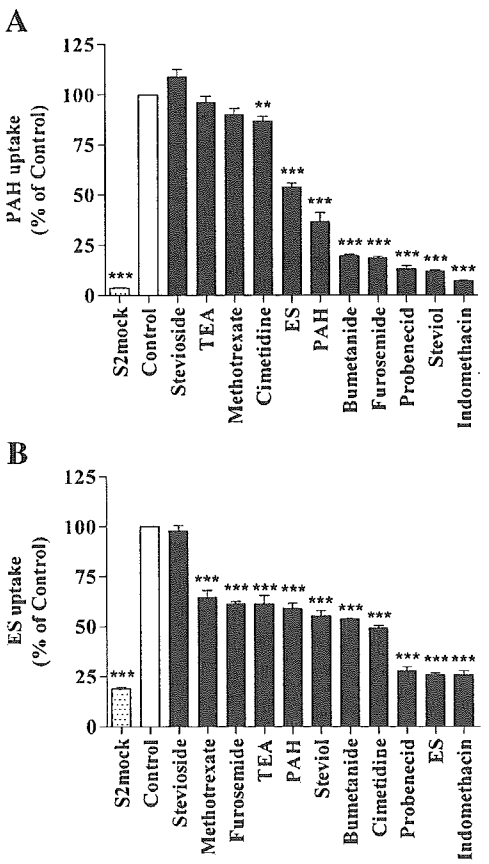

Fig. 3. The inhibitory profiles of stevioside, steviol, and various compounds on [^{14}C]-PAH and [^{3}H]-ES uptake mediated by S2 cells expressing hOAT1 (A) and hOAT3 (B). S2hOAT1 and S2hOAT3 cells were incubated for 2 min in D-PBS containing 5 μM of [^{14}C]-PAH (hOAT1) and 50 nM of [^{3}H]-ES (hOAT3) in the absence (control) or presence of 100 μM of the compounds. Each value represents the mean ± SE from three separate experiments. Mean control PAH and ES uptake were 65.0 ± 1.8 and 0.4 ± 0.1 pmol mg protein^{-1} min^{-1}, respectively. *p < 0.05, **p < 0.01, ***p < 0.001 *vs.* control.